Copyright Warning & Restrictions

The copyright law of the United States (Title 17, United States Code) governs the making of photocopies or other reproductions of copyrighted material.

Under certain conditions specified in the law, libraries and archives are authorized to furnish a photocopy or other reproduction. One of these specified conditions is that the photocopy or reproduction is not to be "used for any purpose other than private study, scholarship, or research." If a, user makes a request for, or later uses, a photocopy or reproduction for purposes in excess of "fair use" that user may be liable for copyright infringement,

This institution reserves the right to refuse to accept a copying order if, in its judgment, fulfillment of the order would involve violation of copyright law.

Please Note: The author retains the copyright while the New Jersey Institute of Technology reserves the right to distribute this thesis or dissertation

Printing note: If you do not wish to print this page, then select "Pages from: first page # to: last page #" on the print dialog screen

FAILURE SURFACE FOR L-SHAPED REINFORCED CONCRETE SHORT COLUMNS

by

Mon-Chen Liu

Thesis submitted to the Faculty of the Graduate School of the New Jersey Institute of Technology in partial fulfillment of the requirements for the degree of Master of Science in Civil Engineering

1983

APPROVAL SHEET

Title of Thesis: Failure Surface for L-shaped Reinforced Concrete Short Columns

Name of Candidate: Mon-Chen Liu, 1983
Master of Science in Civil Engineering

Thesis and Abstract Approved: _____ _____

Dr. C.T. Thomas Hsu
Assistant Professor
Department of Civil and
Environmental Engineering

Signatures of other members of the thesis committee. _____ _____

_____ _____

VITA

Name: Mon-Chen Liu

Degree and date to be conferred: MSCE, 1983

Collegiate institutions attended

	Dates	Degree	Date of Degree
National Central University	1973-1977	BSCE	June 1977
New Jersey Institute of Technology	1982-1983	MSCE	May 1983

Major: Civil Engineering

ABSTRACT

Title of Thesis: Failure Surface for L-shaped Reinforced Concrete Short Columns

Mon-Chen Liu, Master of Science in Civil Engineering, 1983

Thesis directed by: Dr. C.T. Thomas Hsu
Assistant Professor
Department of Civil and
Environmental Engineering

Combined bending and axial compression for L-shaped reinforced concrete short columns is a common problem. But the present ACI Building Code (ACI 318-77), handbooks and texbooks pay no attention to this problem. A numerical analysis and computer program developed by Hsu for a reinforced concrete member subject to biaxial bending and axial load has been used. Using this computer program, the interaction diagrams and failure surface were developed for L-shaped members under combined bending and axial compression. A comparison between theoretical and experimental results was included to examine the validity of failure surface.

ACKNOWLEDGEMENTS

I would like to express my sincerest gratitude to my advisor Dr. C.T. Thomas Hsu, who not only set up the topic for me, but also always gives me more than enough helps, guidances and encouragemen ughout the whole period of this work. Writing this thesis gave me a great opportunity of education both from Dr. C.T. Thomas Hsu and the topic itself.

I would also like to thank those professors from the Civil and Environmental Department for their help during the years I was attending the Graduate School at the New Jersey Institute of Technology.

Last of all, I would like to thank my lovely wife who proofread and typed this paper.

TABLE OF CONTENTS

CHAPTER I

GENERAL INTRODUCTION AND SCOPE OF INVESTIGATIONS

The objective of this study is to investigate the interaction diagrams and failure surface for reinforced concrete short columns with L-shaped cross-section subject to combined uniaxial or biaxial bending and axial compression. Also, the non-linear behavior of the moment-curvature characteristics for L-shaped cross section is studied under these combined loadings. Besides, experimental tests and numerical results are compared to examine the validity of the computer analysis developed.

The present ACI Building Code (ACI 318-77) (1), handbooks (2,3), texbooks (4,5,6) and design aids are adequate enough for use in designing members with standard cross sections under combined bending (uniaxial or biaxial) and axial compression. But unfortunately, all these aids were developed for the symmetrical section such as rectangular, square, and circular sections. The subject of unsymmetrical section (e.g. L-shaped) reinforced concrete member under combined bending and axial load is neither trivial nor undeserving attention. The L-shaped reinforced concrete columns are being used at the reentrant building corners. However, the information for their analysis and design is not generally available to the structural

engineer , either in working stress or ultimate strength theories.

The development of failure surface for the L-shaped reinforced concrete members under combined bending and axial load was previously reported by Marin (7). Marin presented several numerical studies of the strength of L-shaped reinforced concrete short columns subjected to combined axial load and biaxial bending. Three sample design charts were presented in his paper to provide the design aids for the structural engineers. However, there are some limitations in this approach such as the steel distribution for each thickness ratio must be maintained symmetrically. Also, his analysis was not compared with any experimental tests.

A survey of the literature reveals a scarcity of comprehensive analytical and experimental data on the strength and deformation (or moment-curvature) behavior of irregular reinforced concrete member subject to combined loading. The proposed research is based on the basic governing equations of strain compatibility and summation of forces and moments by using numerical analysis. This analysis was developed originally by Hsu (12-17) to study the deformation, strain, curvature and strength behavior

and strength interaction curves for L-shaped reinforced concrete members subjected to uniaxial or biaxial bending and axial compression.

Unlike the symmetrical section, the principal axes do not coincide with the centroidal axes. Therefore, the concepts of coordinate-transformation are provided to overcome this problem. The writer starts with the literature review of both symmetrical and unsymmetrical reinforced concrete cross-section columns under combined bending and axial load. Chapter 2 contains all these reviews and the development of the analysis of reinforced concrete section subject to combined loading. The nonlinear behavior and analysis of reinforced concrete column under combined loadings are presented for both symmetrical and unsymmetrical cross-section. Also the transformation of coordinate systems will be discussed. Besides, the comparisons of theoretical and experimental results for L-shaped reinforced concrete columns are provided by using the moment-curvature diagrams and the three-dimensional failure surfaces.

In Chapter 3, the interaction diagrams for combined bending and axial load are developed from the computer output. Two different maximum concrete compressive stress f_c' have been used for the L-shaped columns. Five sets of interaction diagrams have been furnished for the analysis

purpose. Furthermore, the nondimensional load contours at the constant loads for L-shaped reinforced concrete columns under combined loading are also discussed.

The objective of this chapter is to investigate into the strength interaction curves of reinforced concrete columns under combined bending and axial compression as the applied load is increased monotonically from zero load until the ultimate strength obtained.

The objective of Chapter 4 is to compared the theoretical failure surface with the experimental tests by the other graduate students at the New Jersey Institute of Technology. All of these analyses and findings are concluded in Chapter 5.

CHAPTER II

A LITERATURE REVIEW OF LOAD-MOMENT-CURVATURE RELATIONSHIPS FOR L-SHAPED REINFORCED CONCRETE COLUMN SECTIONS

2-1 A REVIEW OF BIAXIAL BENDING AND COMPRESSION FOR RECTANGULAR OR SQUARE SECTION

The investigation or design of a square or rectangular section subject to an axial compression in combination with bending moments about both the X and Y axes has received considerable attention. These method essentially involves a trial and error process for obtaining the position of an inclined neutrul axes; hence any such method is sufficiently complex that no formula may be developed for practical use.

The concept of using failure surfaces has been presented by Bresler (11) and Pannell (18). The theoretical ultimate strength of a section is a function of three variables, P_n, M_{nx}, and M_{ny}, which may also be expressed in terms of the axial force P_n acting at eccentricities $e_y = M_{nx} / P_n$ and $e_x = M_{ny} / P_n$ with respect to the X and Y axes. Three types of failure surfaces may be defined. In the first type S_1, the variables used along the three orthogonal axes are P_n, e_x, and e_y, as shown in Fig. 2-1-1, in the second type S_2, the variables are $1 / P_n$, e_x, e_y, as shown in Fig. 2-1-2; and in the third type S_3, the variables are P_n, M_{nx}, and M_{ny}, as

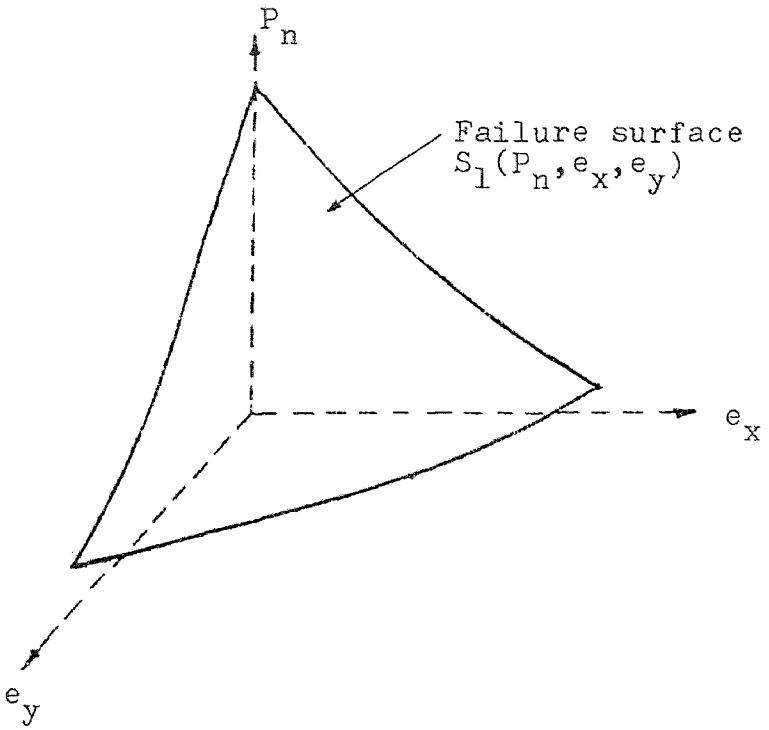

Fig. 2-1-1 FAILURE SURFACE $S_1(P_n, e_x, e_y)$

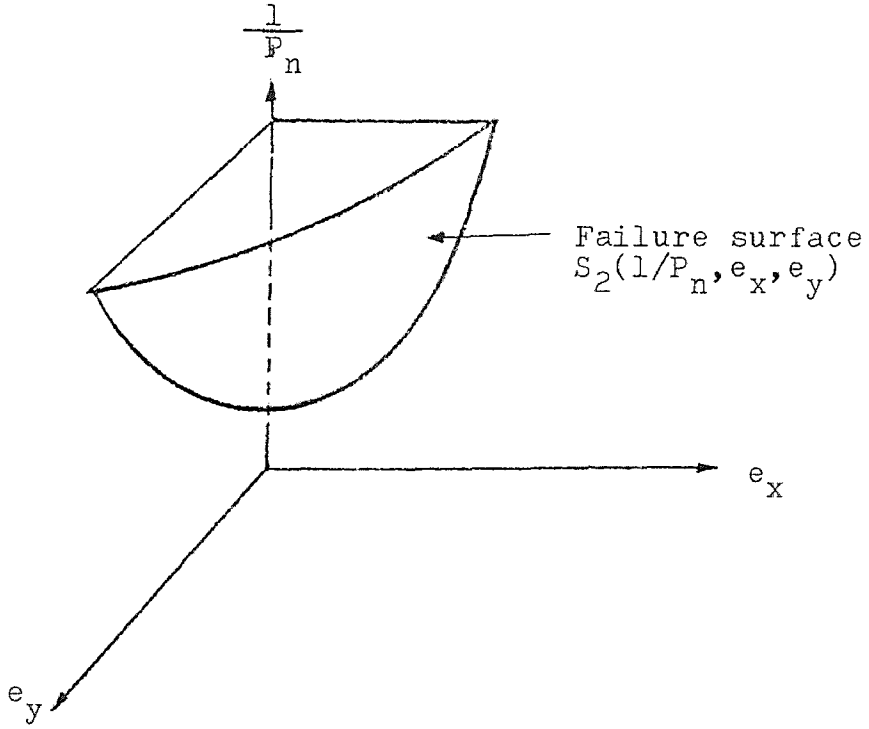

Fig. 2-1-2 RECIPROCAL FAILURE SURFACE $S_2(1/P_n, e_x, e_y)$

shown in Fig. 2-1-3.

Bresler has developed a very useful analysis procedure (11) using the reciprocal surface S_2. The third type of failure surface S_3 is a three-dimensional extension of the interaction diagram for combined loading. A number of investigators have made approximations to S_3 for use in design and analysis (11,19,20,21,22). Bresler (11) and Parme, Nieves, and Gouwens (22) have suggested practical approaches to the use of the surface S_3. In summary, two analysis methods are used: the first using the reciprocal $1 / P_n - e_x - e_y$ surface S_2 that gives a simple tool for analysis, and the second using the $P_n - M_{nx} - M_{ny}$ surface S_3 which is very helpful in design.

2-1-1 BRESLER RECIPROCAL LOAD METHOD :

When the inverse of the failure load, $1 / P_n$, is plotted on one axis and the eccentricities. e_x and e_y of the two major axes on the other two axes, as shown in Fig. 2-1-4, the approximate equation for this failure surface is :

$$\frac{1}{P_i} = \frac{1}{P_x} + \frac{1}{P_y} - \frac{1}{P_0} \qquad (2\text{-}1)$$

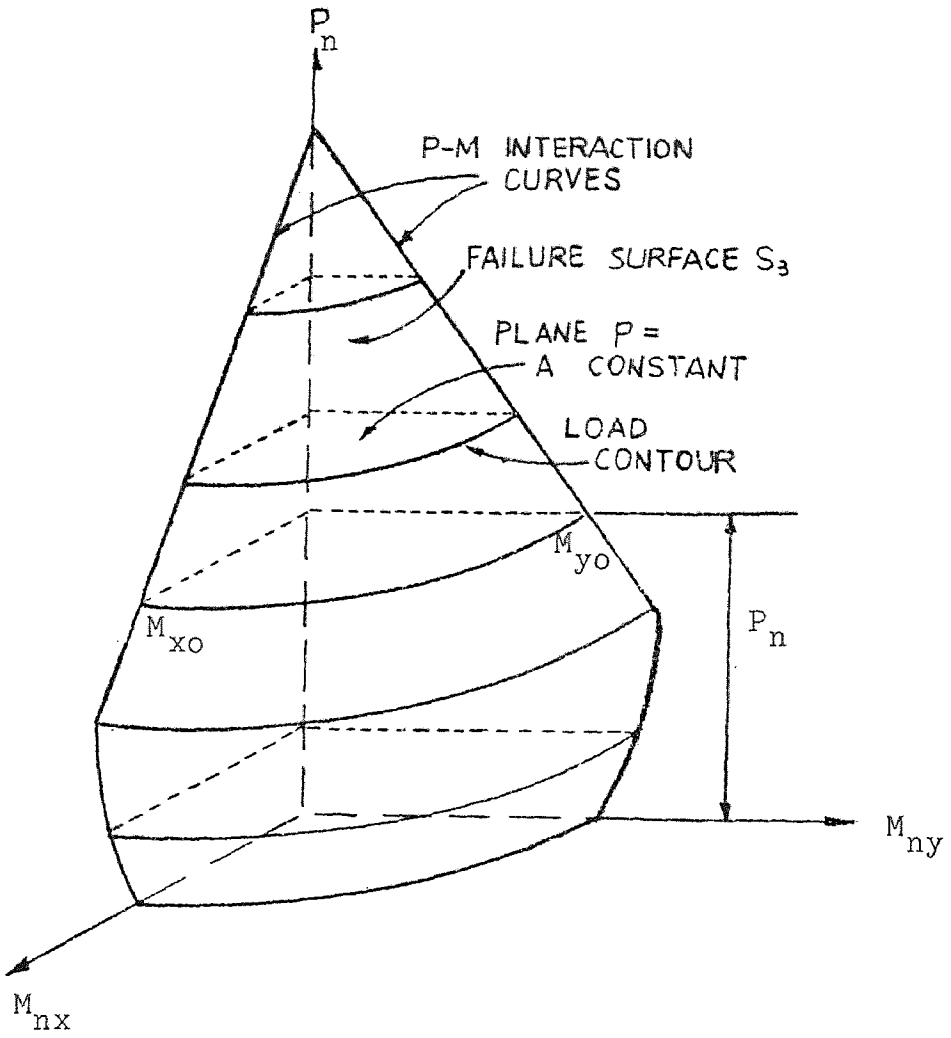

Fig. 2-1-3 FAILURE SURFACE $S_3(P_n, M_{ny}, M_{nx})$

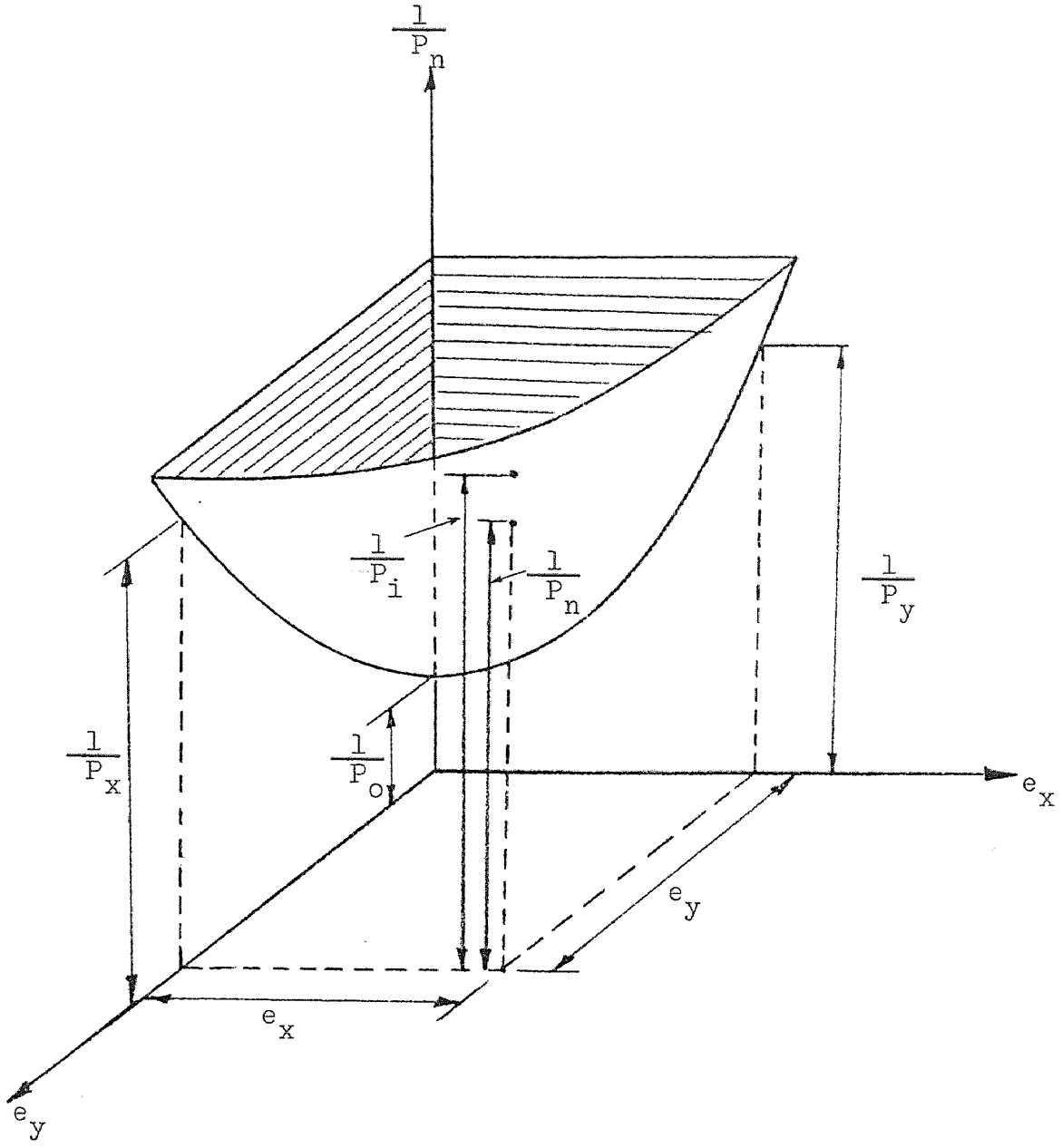

Fig. 2-1-4 FAILURE SURFACE $(1/P_n, e_x, e_y)$ THE RECIPROCAL LOAD METHOD

where

P_i = Approximate load capacity of the section (i.e. $P_i \doteq P_n$) when subjected to eccentricities e_x and e_y

P_x, P_y = Load-carrying capacities of the section under compression with uniaxial eccentricity e_x and e_y, respectively

P_o = Load-carring capacity of the section under eccentric axial compression

Bresler has found the computed values of P_i from Eq. (2-1) to be " in excellent agreement with test results, the maximum deviation being 9.4%, and the average deviation being 3.3% ". Ramamurthy (21) also reported test results and concluded that Eq. (2-1) " can be used to predict ultimate loads with reasonable accuracy ". However, Pannell has presented additional test results and indicated that Eq. (2-1) may be inappropriate when small values of axial load are involved, such as when P_n / P_o is in the range of 0.06 or less.

2-1-2 LOAD CONTOUR METHOD — BRESLER APPROACH

Bresler described another failure surface which is shown in Fig. 2-1-3. The failure thrust is plotted against the associated failure moments, M_{nx} and M_{ny},

about two major axes. At a level of axial load, P_n, the failure moments corresponding to that can be related as:

$$\left(\frac{M_{nx}}{M_{ox}}\right)^{\alpha_1} + \left(\frac{M_{ny}}{M_{oy}}\right)^{\alpha_2} = 1.0 \qquad (2\text{-}2)$$

where:

M_{nx}, M_{ny} = monents at failure load, P_n, about X-axis and Y-axis, respectively

M_{ox} = failure moment about X-axis when axial load, P_n, acts with uniaxial eccentricity producing moment about the X-axis only (i.e. $M_{ny} = 0$)

M_{oy} = failure moment about Y-axis when axial load, P_n, acts with uniaxial eccentricity producing moment about the Y-axis only (i.e. $M_{nx} = 0$)

α_1 , α_2 = exponents depending on column cross-section dimensions, amount and distribution of steel and properties of concrete

Bresler tested some specimens and made calculations to evaluate the validity of proposed equations. He found that for rectangular sections, α_1 and α_2 in Eq. (2-2) could be assumed equal, so Eq. (2-2) becomes

$$\left(\frac{M_{nx}}{M_{ox}}\right)^{\alpha} + \left(\frac{M_{ny}}{M_{oy}}\right)^{\alpha} = 1 \qquad (2\text{-}3)$$

with α varied from 1.15 to 1.55. For practical purposes, it seems good to take α as 1.5 for rectangular sections and between 1.5 and 2.0 for square sections.

2-1-3 PANNELL CONCEPT OF FAILURE SURFACE

Pannell (18) showed that an interaction surface at any load level, P_n, of a rectangular section columns, as shown in Fig. 2-1-5 (a), could be transformed into an equivalent interaction surface of a square section. If the interaction surface in Fig. 2-1-5 (a) is distorted by multiplying the minor axis coordinate (i.e. M_{nx} in Fig. 2-1-5 (a)) by the ratio M_{oy} / M_{ox}, then it will transfer to coincide with the interaction surface of square sections in Fig. 2-1-5 (b), where M_{oy} and M_{ox} are the uniaxial failure moments at load P_n eccentric about the major and minor axes, respectively.

It was also confirmed that the ratio of M_{oy} / M_{ox} at load levels for the cross section was effectively a constant and might be represented by the ratio $\phi = M_{by} / M_{bx}$ of " balanced" failure moments about the major and minor axes. When the square column interaction surface is used, it is possible to calculate the failure moment about the diagonal, M_d. With three points, M_{oy}, M_d, and ϕM_{ox} in Fig. 2-1-6, Pannell drew a smooth continuous curve " A " tangent to these points and use the curve to define the

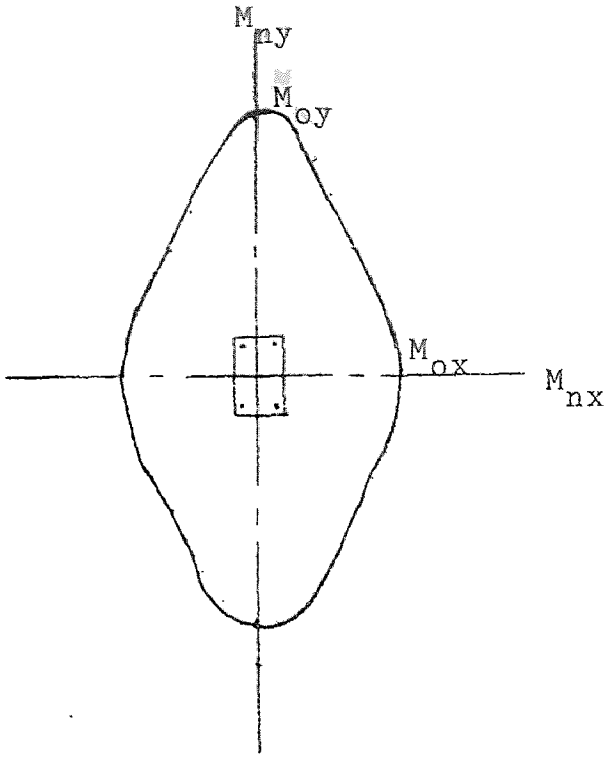

Fig. 2-1-5a INTERACTION DIAGRAM AT CONSTANT LOAD FOR RECTANGULAR COLUMN

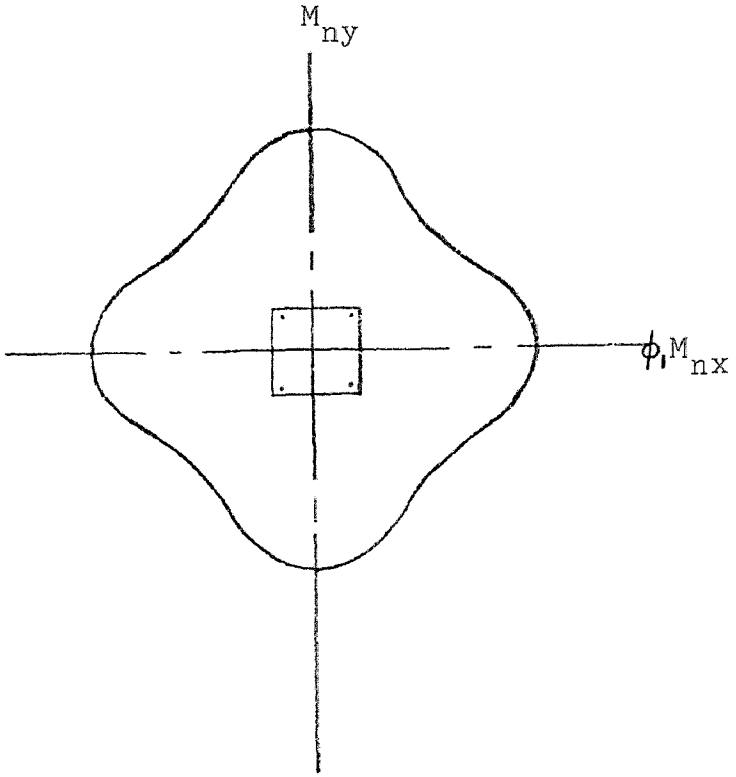

Fig. 2-1-5b INTERACTION DIAGRAM AT CONSTANT LOAD FOR SQUARE COLUMN

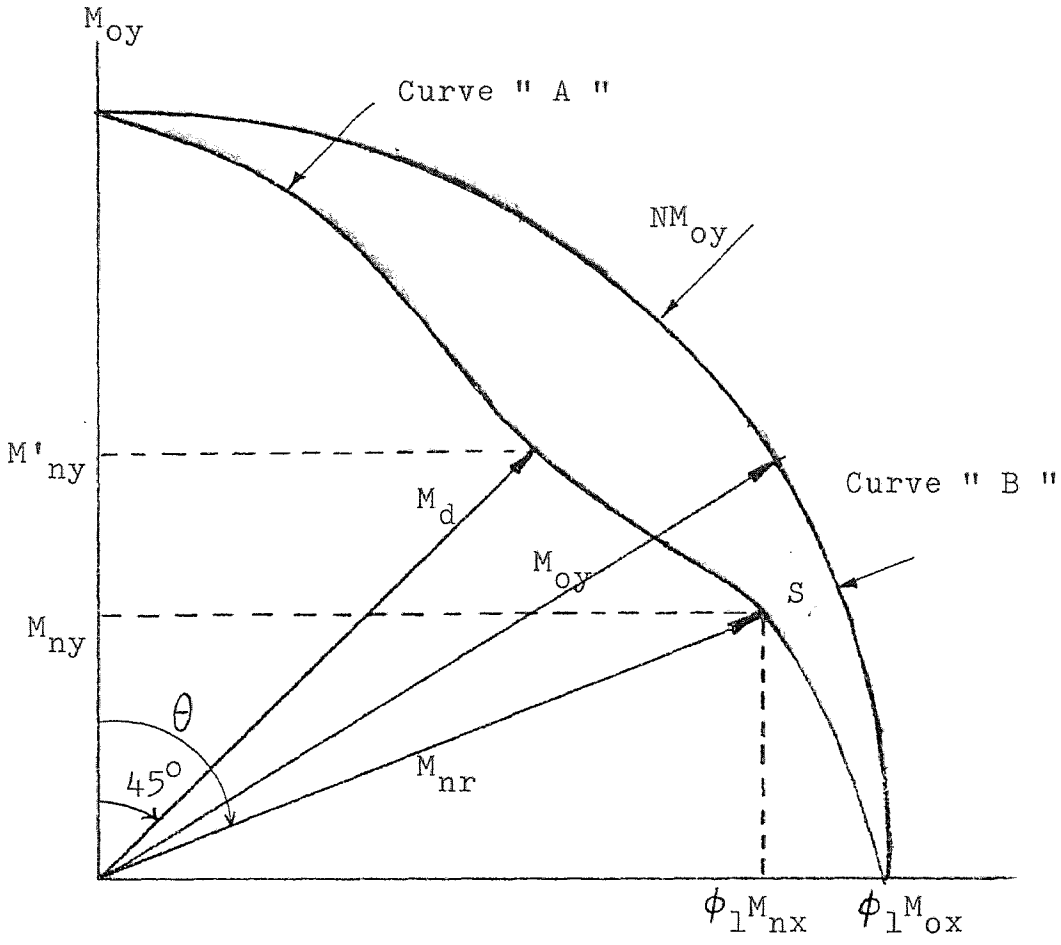

Fig. 2-1-6 HORIZONTAL SECTION OF QUADRANT OF ACTUAL FAILURE SURFACE AND SURFACE OF REVOLUTION

entire failure surface.

Also in Fig. 2-1-6 is the circular arc " B " which resulted from revolving the uniaxial failure moment, M_{oy}, about the origin. At the load angle of 45^{o}, the deviation from the diagonal failure moment, M_d, to the circular arc can be found as $M_{oy}-M_d$ or NM_{oy}, where $N = 1 - M_d / M_{oy}$. Pannell gave the equation of the deviation " S " of curve " A " to the circular arc " B " as:

$$S = NM_{oy}Sin^{2}\theta \qquad (2-4)$$

where θ is the load angle.

At any point on the failure surface " A " with the load P_n and resulting moment M_{nr} of $\phi_1 M_{nx}$ and M_{ny}, Pannell showed that the required uniaxial moment capacity is:

$$M_{oy} = \frac{M_{ny}Sec\theta}{1-NSin^{2}\theta} \qquad (2-5)$$

in which $\theta = \tan^{-1} \dfrac{\phi_1 M_{nx}}{M_{ny}}$

Pannell also included a chart for the value of N calculated from the basic equation of equilibrium of the section (18). He tried to compare his method with

Bresler's load contour equation (Eq. 2-3) by rewriting the equation in the form as follows:

$$\left(\frac{M_{nx}}{M_{ox}}\right)^{\alpha} + \left(\frac{M_{ny}}{M_{oy}}\right)^{\alpha} = 1$$

$$\left(\frac{\phi M_{nx}}{M_{oy}}\right)^{\alpha} + \left(\frac{M_{ny}}{M_{oy}}\right)^{\alpha} = 1$$

$$(M_{oy})^{\alpha} = (\phi M_{nx})^{\alpha} + (M_{ny})^{\alpha} \qquad (2\text{-}6)$$

After the comparison, Pannell concluded that his proposed Eq. 2-5 gave better accuracy than Eq. 2-6 and was easier to use. The exponent α of Eq. 2-6 was difficult to determine because it varied within a wide range and it was sensitive to the condition of eccentricity. Pannell also claimed that his method was practical for design, because only one major axis interaction curve was needed.

Besides, there are more simplifications were made for interaction failure surface. However, all of these simplifications are limited to symmetrical cross-section columns. In the future, the writer will extend the load contour surfaces to those of L-shape reinforced concrete columns with L-shaped cross section.

2-2 MARIN'S FAILURE SURFACES

In 1979 Marin used the isoload strength method to develop the design charts for L-shaped sections reinforced

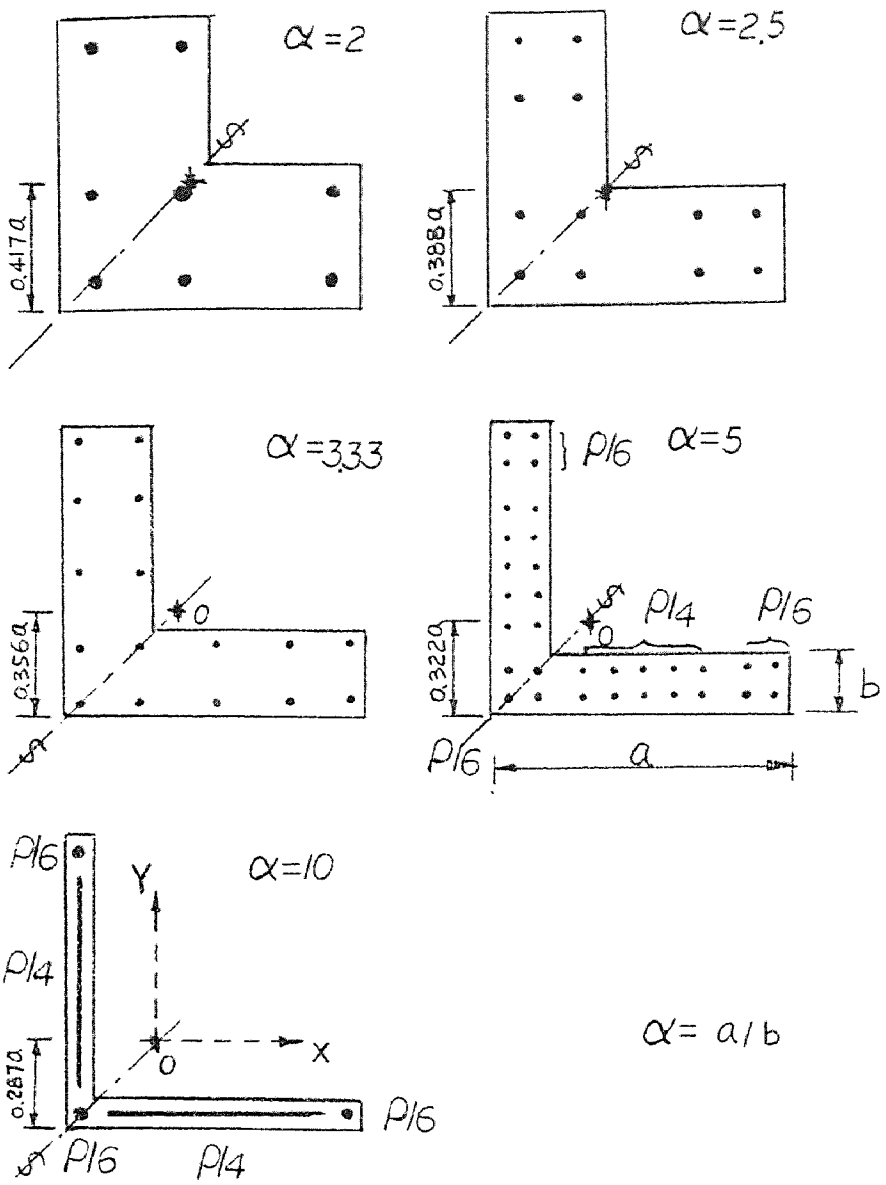

Fig. 2-2-1 THICKNESS RATIO AND CENTROID OF GROSS AREAS FOR L-SHAPED SECTION

concrete column (7). The concrete cross sections were considered symmetrical. Five thickness ratio were selected for the L-shaped columns and the centroid of gross L-shaped section areas are chosen as shown in Fig. 2-2-1. In order to reduce the number of charts to the minimum, the steel distributions were chosen as shown in Fig. 2-2-1. Also, some basic parameters were selected among these five cases, these included the increment of specific axial load level ν and the mechanical ratio ω (where $\nu = P_u / 0.85f_c'A_g$ and $\omega = \rho f_y / 0.85f_c'$). The steps for computational procedure are given as follows:

1. Find the specific axial load and bending moments.
2. Locate the available isoloads in the proper thickness ratio chart closest to the computed ν.
3. Use the values in step 1, find the corresponding mechanical ratio ω and interpolate for ν.

Further details can be found in reference 7.

2-3 NONLINEAR BEHAVIOR AND ANALYSIS OF REINFORCED CONCRETE COLUMNS UNDER COMBINED LOADINGS

2-3-1 LOAD-MOMENT-CURVATURE RELATIONSHIPS:

A modification of the extended Newton-Raphson method (23,24,25) was developed for the determination of strain and curvature distributions in reinforced concrete section subjected to biaxial bending moments and axial compression

(12-17). The cross-section is divided into several small elemental areas and for a given section the stress resultants P, M_x, and M_y can be expressed as functions of curvatures ϕ_x, ϕ_y, and strain ϵ_p as follows:

$$P = P(\phi_x, \phi_y, \epsilon_p) \tag{2-7a}$$

$$M_x = M_x(\phi_x, \phi_y, \epsilon_p) \tag{2-7b}$$

$$M_y = M_y(\phi_x, \phi_y, \epsilon_p) \tag{2-7c}$$

A small element K with its centroid at point (X_k, Y_k) is referred to the principal axes (Fig. 2-3-1). The strain ϵ_k is considered to be uniform all over the small element K and since plane sections remain plane during bending, the strain ϵ_k is given as:

$$\epsilon_k = \epsilon_p + \phi_x Y_k + \phi_y X_k \tag{2-8}$$

Hsu had modified Cranston and Chatterji's stress-strain curves for the concrete as shown in Fig. 2-3-2 (13). These curves account for the strain-softening of concrete and the values of ultimate compressive strain in unconfined and confined concrete elements. The ultimate tensile stress is $0.25f_t''$ (f_t'' is the tensile stress in concrete which equals to 500psi). The tensile strain is

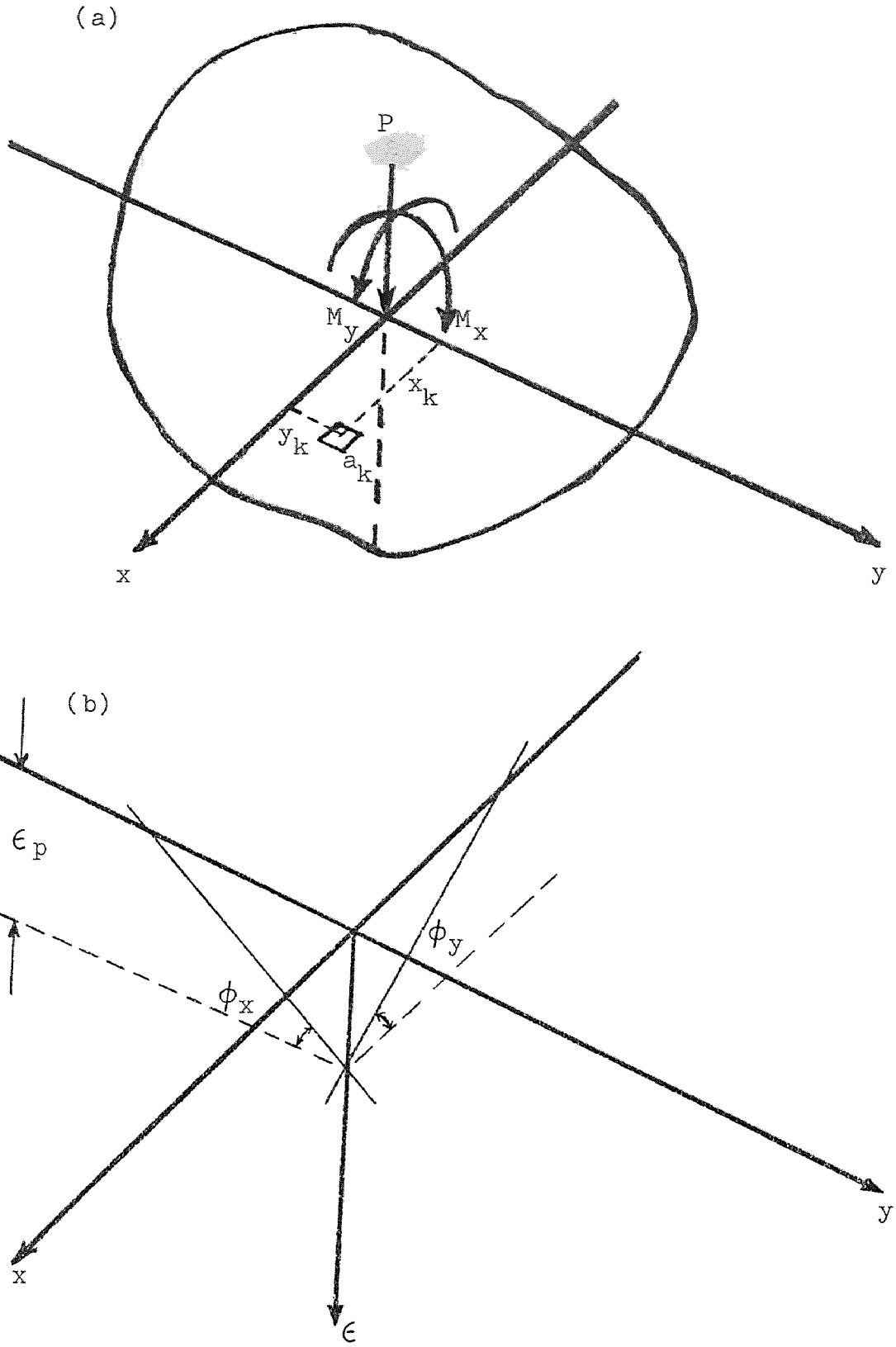

Fig. 2-3-1 IDEALIZATION OF A CROSS-SECTION SUBJECTED TO BIAXIAL BENDING AND AXIAL LOAD

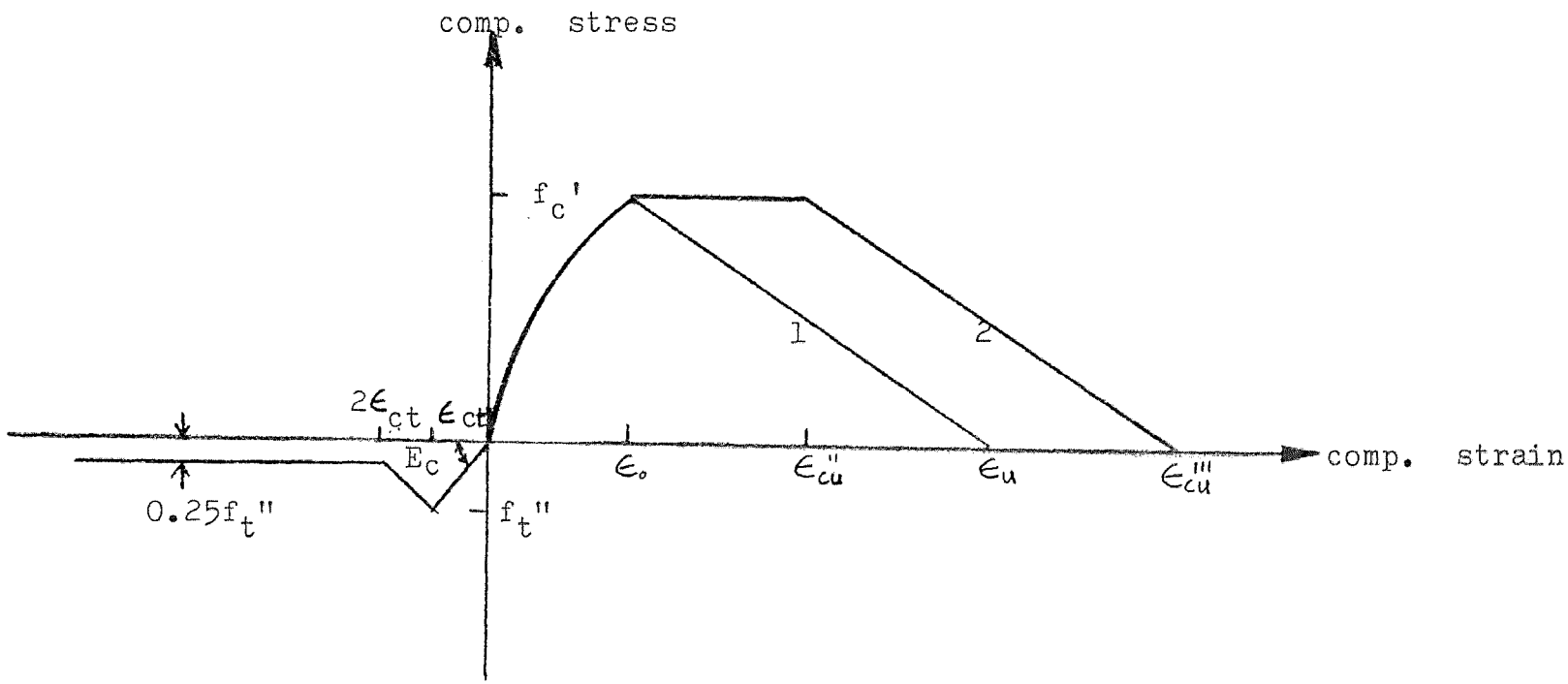

1: Unconfined concrete

2: Confined concrete

Fig. 2-3-2 CONCRETE STRESS-STRAIN CURVES

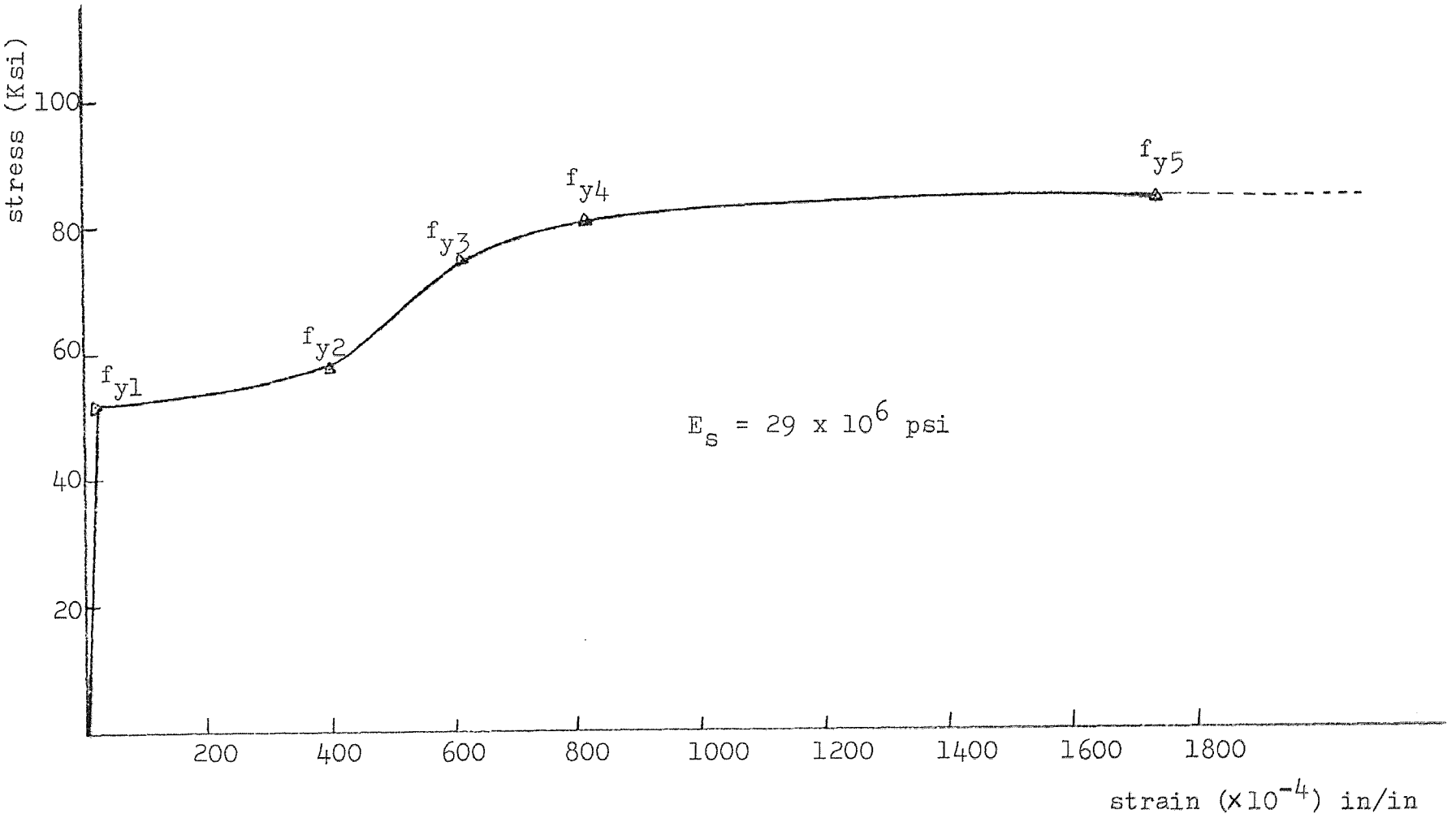

Fig. 2-3-3 STEEL STRESS-STRAIN CURVE

not limited. The stress-strain curve for steel has been idealized using the peice-wise linear approximation with the modulus of elasticity E_s as 29,000,000psi in the strain hardening region as shown in Fig. 2-3-3.

Once the strain distribution across the cross-section is established, the axial load P and bending moment M_x and M_y can be calculated using the following equations:

$$P_{(c)} = \sum_{k=1}^{n} f_k a_k \tag{2-9a}$$

$$M_{x(c)} = \sum_{k=1}^{n} f_k a_k y_k \tag{2-9b}$$

$$M_{y(c)} = \sum_{k=1}^{n} f_k a_k x_k \tag{2-9c}$$

where the subscript (c) means calculated values of P, M_x, and M_y, which is obtained in an iteration cycle; a_k is the area of element k with its centroid at point (x_k, y_k) and f_k is the uniform stress across the element k. Once knowing $P_{(c)}, M_{x(c)}, M_{y(c)}$ and the corresponding values of $\phi_x, \phi_y, \epsilon_p$ during and iteration cycle, Eq. (2-7) can be expanded by using Taylor's theorem. Neglecting the second and higher order terms, one obtains:

$$P_{(s)} = P_{(c)} + \frac{\partial P_{(c)}}{\partial \phi_x}\delta\phi_x + \frac{\partial P_{(c)}}{\partial \phi_y}\delta\phi_y + \frac{\partial P_{(c)}}{\partial \epsilon_p}\delta\epsilon_p \tag{2-10a}$$

$$M_{x(s)} = M_{x(c)} + \frac{\partial M_{x(c)}}{\partial \phi_x}\delta\phi_x + \frac{\partial M_{x(c)}}{\partial \phi_y}\delta\phi_y + \frac{\partial M_{x(c)}}{\partial \epsilon_p}\delta\epsilon_p \quad (2\text{-}10b)$$

$$M_{y(s)} = M_{y(c)} + \frac{\partial M_{y(c)}}{\partial \phi_x}\delta\phi_x + \frac{\partial M_{y(c)}}{\partial \phi_y}\delta\phi_y + \frac{\partial M_{y(c)}}{\partial \epsilon_p}\delta\epsilon_p \quad (2\text{-}10c)$$

For numerical analysis, these partial derivatives in equations (2-10) are replaced by the corresponding difference quotients. By suitably incrementing one deformation quantity at a time the rates of change can be evaluated and substituted in equation (2-10). The resulting simultaneous equations are solved for $\delta\phi_x$, $\delta\phi_y$ and $\delta\epsilon_p$ and these increments are added to the initial deformation. The process is repeated by using the new deformation values until convergence is obtained.

Let

$$u = P_{(c)} - P_{(s)}$$

$$v = M_{x(c)} - M_{x(s)}$$

$$w = M_{y(c)} - M_{y(s)}$$

Then equation (2-10) can be written in matrix form as:

$$\begin{Bmatrix} u \\ v \\ w \end{Bmatrix} = \begin{bmatrix} \sum_{k=1}^{n} (E_t)_k a_k, & \sum_{k=1}^{n} (E_t)_k a_k y_k, & \sum_{k=1}^{n} (E_t)_k a_k x_k \\ & \sum_{k=1}^{n} (E_t)_k a_k y_k^2, & \sum_{k=1}^{n} (E_t)_k a_k x_k y_k \\ \text{Symmetric} & & \sum_{k=1}^{n} (E_t)_k a_k x_k^2 \end{bmatrix} \begin{Bmatrix} \delta\epsilon_p \\ \delta\phi_x \\ \delta\phi_y \end{Bmatrix} \quad (2\text{-}11)$$

Where $(E_t)_k$ is the tangent modulus of elasticity for steel or concrete in element K, at a given strain level. The values of u,v,w can be selected to suit the accuracy required for values $\delta\phi_x$, $\delta\phi_y$, and $\delta\epsilon_p$. The curvatures ϕ_x, ϕ_y and strain ϵ_p will be adjusted to produce changes δP, δM_x, and δM_y, respectively, until the given load P, M_x and M_y are obtained within the specified tolerances. Once this is achiveved, the computer analysis will go to the next loading level and repeat the entire procedure.

2-3-2 BASIC ASSUMPTIONS FOR HSU'S APPROACH:

In order to apply Hsu's computer program to the reinforced concrete column under biaxial or uniaxial bending and axial compression, the following assumptions have been made in Hsu's investigation.

(1) The bending moment are applied about the principal axes.

(2) Plane sections remain plane after bending.

(3) The longitudinal stress at an element is dependent only on the longitudinal strain at that point.

(4) The stress-strain curves for the concrete and steel are known and there is perfect bond between the concrete and steel.

(5) Strain reversal does not occur.

(6) The effect of creep and shrinkage are ignored.

(7) The member does not buckle before the ultimate load is attained.

2-3-3 CONVERGENCE CRITERIA

The computation will be terminated if the coefficient of the matrix in equation (2-11) becomes zero or negative. convergence of the procedures to calculate the curvatures and the axial strain corresponding to a given axial load and moments is dependent upon the validity of equations (2-8) and (2-11). If the stiffness of section is too small, the procedures will not reach a solution.

The computer program was extend in order to apply to the L-shaped column under combined loadings by the writer. The program is written in FORTRAN IV language and the flow chart is shown in Fig. 2-3-4.

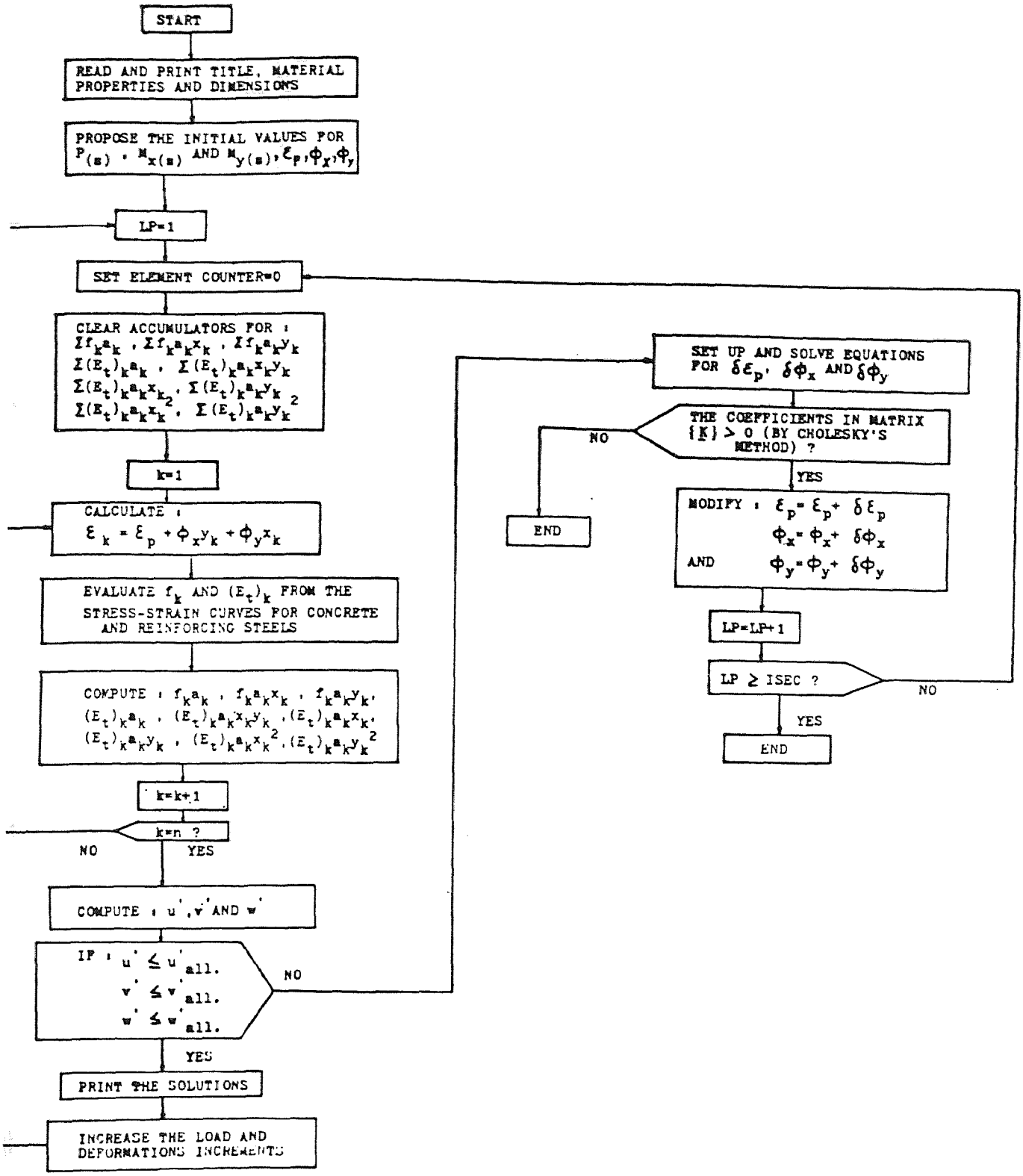

Fig. 2-3-4 FLOW CHART (FROM Ref.13)

2-4 THE COMPARISON BETWEEN THEORETICAL AND EXPERIMENTAL RESULTS

2-4-1 SPECIMEN DESCRIBTION

In order to use Hsu's computer program one has to use the principal axes of the section for analysis. Several specimens have been tested by other graduate students. Here, the writer chooses some of the specimen for comparison. The cross-section of this specimen is shown in Fig. 2-4-1. This cross-section is the same as the column tested by Taghehchian, Yekta and Majlesi (26). The section is divided into 126 elements --- 14 for steel elements, and 50 for unconfined concrete elements, others are the confined concrete elements. Each steel element consists of one No. 3 steel bar (0.11 $in.^2$). Special 1/4 in. diameter bar (As" = 0.025 $in.^2$) are used as ties, and spacing of ties is 3 in.. The ultimate compressive stress for concrete f_c' is 3756psi. The eccentricities of axial load are e_x = 0.643 in. and e_y = 0.643 in.. The other data for this cross-section are shown as follows: (refer to Fig. 2-3-2, Fig. 2-3-3)

f_{y1} = 51800 psi	ϵ_{y1} = 0.0019 in/in
f_{y2} = 57567 psi	ϵ_{y2} = 0.041 in/in
f_{y3} = 74840 psi	ϵ_{y3} = 0.061 in/in
f_{y4} = 80589 psi	ϵ_{y4} = 0.082 in/in

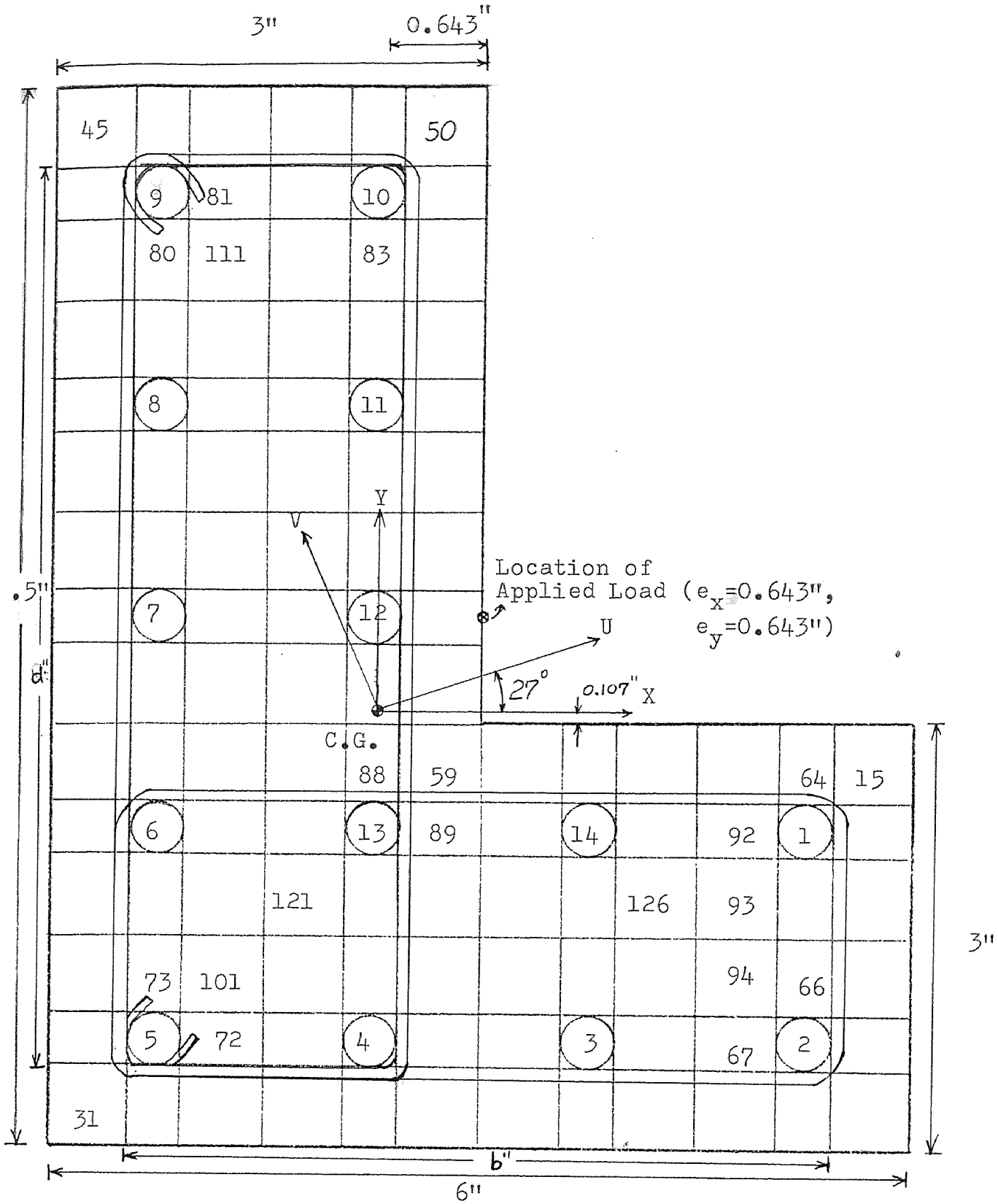

Fig. 2-4-1 L-SHAPED COLUMN SECTION

f_{y5} = 83764 psi ϵ_{y5} = 0.1734 in/in

f_{y1}' = 51800 psi ϵ_{y1}' = 0.0019 in/in

f_{y2}' = 57567 psi ϵ_{y2}' = 0.041 in/in

f_{y3}' = 74840 psi ϵ_{y3}' = 0.061 in/in

f_{y4}' = 80589 psi ϵ_{y4}' = 0.082 in/in

f_{y5}' = 83764 psi ϵ_{y5}' = 0.1734 in/in

f_c' = 3756 psi S = 3.0 in

A_s'' = 0.025 in.^{2} E_c = 1000 f_c'psi

ϵ_o = 0.002 in/in ϵ_u = 0.012 in/in

f_t' = 500 psi

$$\epsilon_{cu}'' = \frac{\sqrt[3]{p'''}}{24.5} + 0.002 \qquad \epsilon_{cu}''' = \frac{\sqrt[3]{p'''}}{4.9} + 0.012$$

$$p''' = \frac{2(b'' + d'')\, A_s''}{b''\, d''\, S}$$

Where S is the spacing of ties, b'' and d'' are shown in Fig. 2-4-1. The stress-strain curves for steel and concrete are shown in Fig. 2-3-2 and Fig. 2-3-3 (Ref. 13).

2-4-2 TRANSFORMATION MATRIX

Since principal axes are taken for analytical purpose, coordinates transformation is an important procedure. From the strength of materials, the following steps can be used as transformation:

(1) Find moment of inertia I_x , I_y and product moment of inertia I_{xy} for this section geometry with

respect to centroidal axes X and Y.

(2) Use equation: $\tan 2\theta = 2I_{xy}/(I_y - I_x)$ to determine the angle θ between centroidal and principal axes.

(3) Use equation: $\begin{Bmatrix} u \\ v \end{Bmatrix} = R \begin{Bmatrix} x \\ y \end{Bmatrix}$,

$$\text{where } R = \begin{bmatrix} \cos\theta & \sin\theta \\ -\sin\theta & \cos\theta \end{bmatrix}$$

Following these steps, the data for this specimen can be determine as:

$I_x = 144.8 \text{ in.}^4$

$I_y = 81.5 \text{ in.}^4$

$I_{xy} = -43.4 \text{ in.}^4$

$\therefore \theta = 27^o$

Since $e_x = 0.643$ in. $\quad e_y = 0.643$ in.

$\therefore \quad e_u = 0.865$ in. $\quad e_v = 0.281$ in.

From the above investigation, the load, moment and curvature with respect to principal axes U, V can be found easily. For practical purpose, these results should be transfered to centroidal axes X and Y.

Now, consider the centroidal axes X, Y as global coordinate and principal axes U, V as structural coordinate as shown in Fig.2-4-2a and Fig.2-4-2b. The angle of rotation is considered as counterclockwise rotates from

(a)

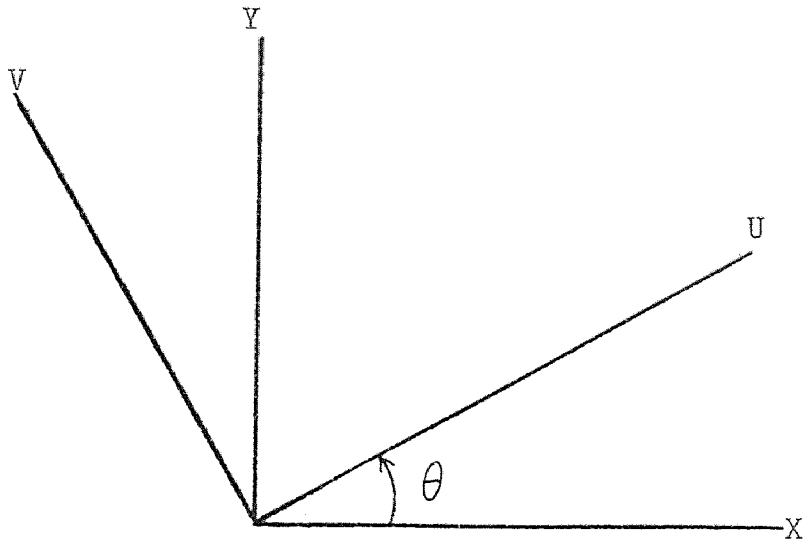

(b)

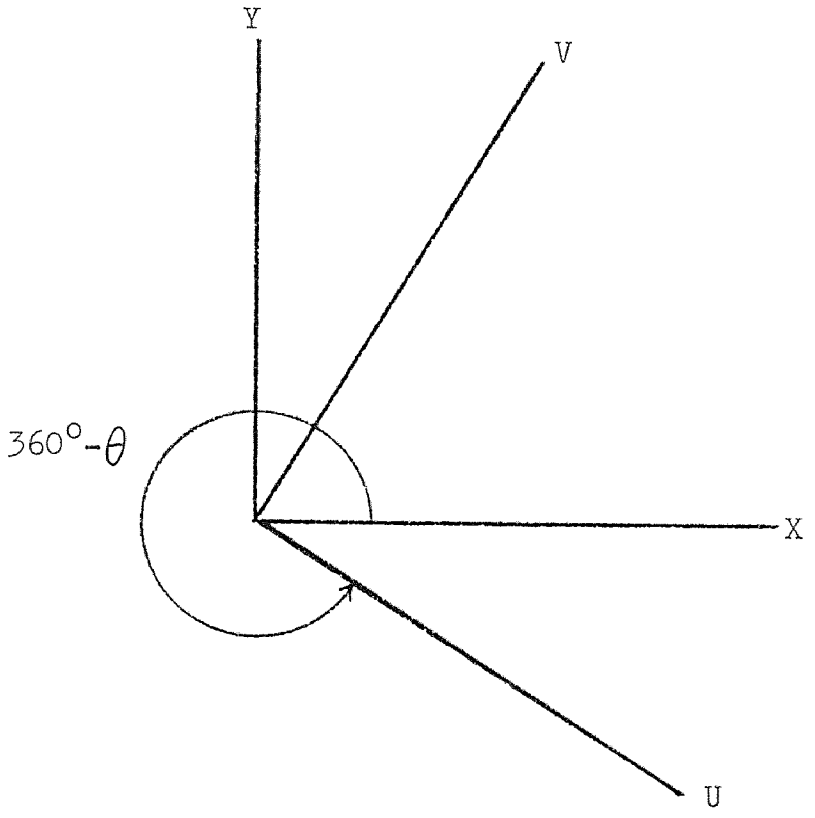

Fig. 2-4-2 TRANSFORMATION OF COORDINATE

global coordinate to structural coordinate. According to this, the coordinates transformation matrix R' can be obtained as follow (see Ref. 16):

(a) For the case in Fig. 2-4-2a:

$$R' = \begin{bmatrix} \cos\theta & \sin\theta \\ -\sin\theta & \cos\theta \end{bmatrix}$$

$$\text{then} \begin{Bmatrix} M_x \\ M_y \end{Bmatrix} = \begin{bmatrix} R' \end{bmatrix} \begin{Bmatrix} M_u \\ M_v \end{Bmatrix}$$

$$\text{and} \begin{bmatrix} \phi_x & \phi_{xy} \\ \phi_{xy} & \phi_y \end{bmatrix} = \begin{bmatrix} R' \end{bmatrix}^T \begin{bmatrix} \phi_u & \phi_{uv} \\ \phi_{uv} & \phi_v \end{bmatrix} \begin{bmatrix} R' \end{bmatrix}$$

(b) For the case in Fig. 2-4-2b:

$$R' = \begin{bmatrix} \cos(360^\circ-\theta) & \sin(360^\circ-\theta) \\ -\sin(360^\circ-\theta) & \cos(360^\circ-\theta) \end{bmatrix} = \begin{bmatrix} \cos\theta & -\sin\theta \\ \sin\theta & \cos\theta \end{bmatrix}$$

$$\text{then} \begin{Bmatrix} M_x \\ M_y \end{Bmatrix} = \begin{bmatrix} R' \end{bmatrix} \begin{Bmatrix} M_u \\ M_v \end{Bmatrix}$$

$$\text{and} \begin{bmatrix} \phi_x & \phi_{xy} \\ \phi_{xy} & \phi_y \end{bmatrix} = \begin{bmatrix} R' \end{bmatrix}^T \begin{bmatrix} \phi_u & \phi_{uv} \\ \phi_{uv} & \phi_v \end{bmatrix} \begin{bmatrix} R' \end{bmatrix}$$

Since U, V are principal axes, in both cases (a),(b) $\phi_{uv} = 0$.

From the above investigation, the ultimate moment and curvature can be transfered to those of the centroidal

axis. These results are also compared with experimental results (26) by plotting on the moment-curvature diagram as shown in table-1, Fig. 2-4-3 and Fig. 2-4-4. Although the theoretical and experimental moment-curvature results are in good agreement, the values of theoretical moment values are higher than those of the experimental ones. This may be attributed to the fact that the experimental moment values is calculated by $M_{nx} = P_n e_y$ and $M_{ny} = P_n e_x$ where δ_x, δ_y, (mid-height deflections) are ignored in computation. The actual experimental moment values should by calculated as follows:

$$M_{nx} = P_n(e_y + \delta_y)$$
$$M_{ny} = P_n(e_x + \delta_x)$$

TABLE-1 ULTIMATE STRENGTH FOR SPECIMEN #4 (Ref. 26)

$e_x = 0.643''$, $e_y = 0.643''$			
	P(Kips.)	M_x(in.-Kips.)	M_y(in.-Kips.)
theoretical	116.5	75.0	75.0
experimental	109.0	70.09*	70.09*

* Mid-height deflections are not included in computing the bending moment (ref. 26)

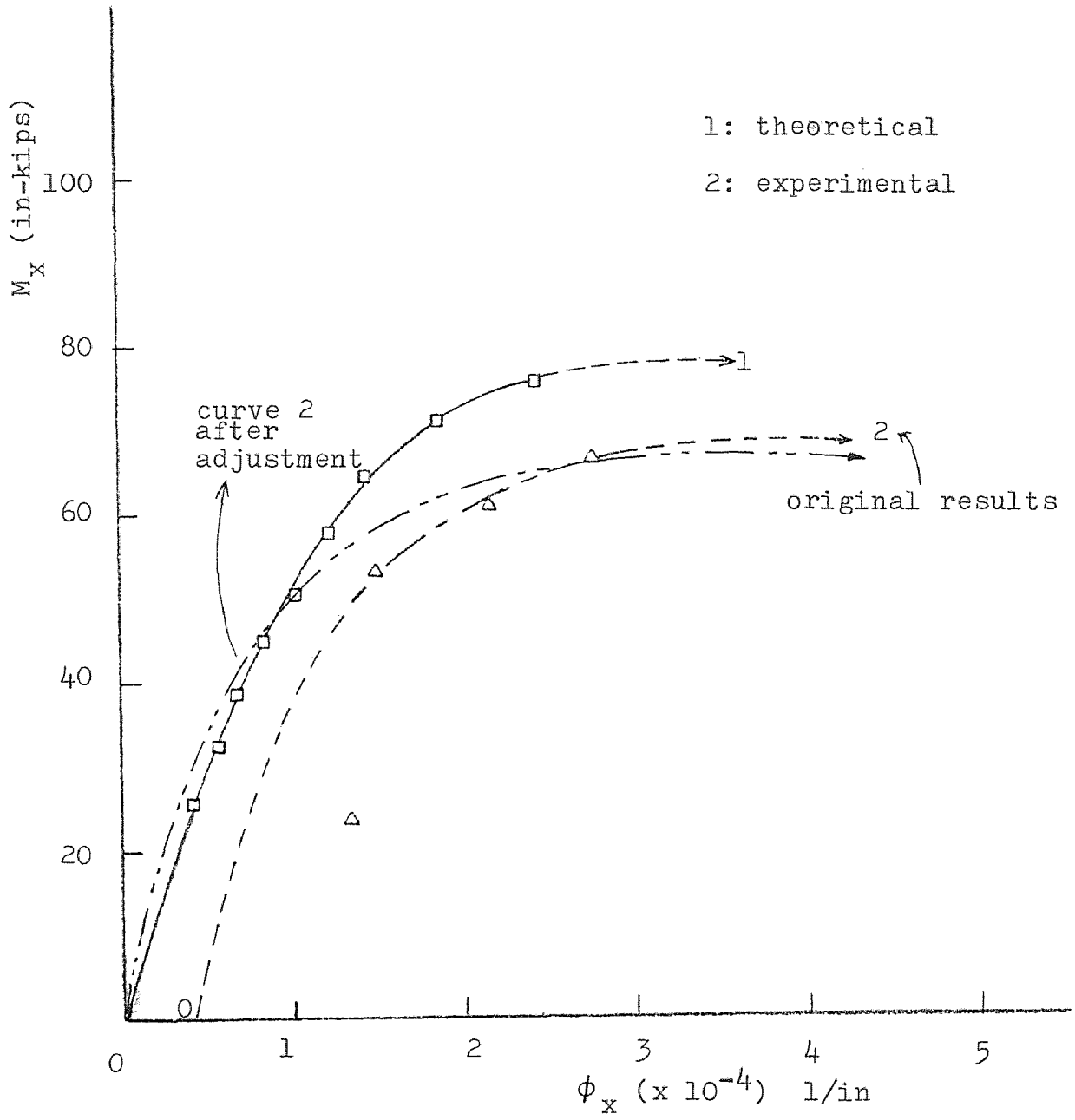

Fig. 2-4-3 MOMENT-CURVATURE DIAGRAM IN X-DIRECTION

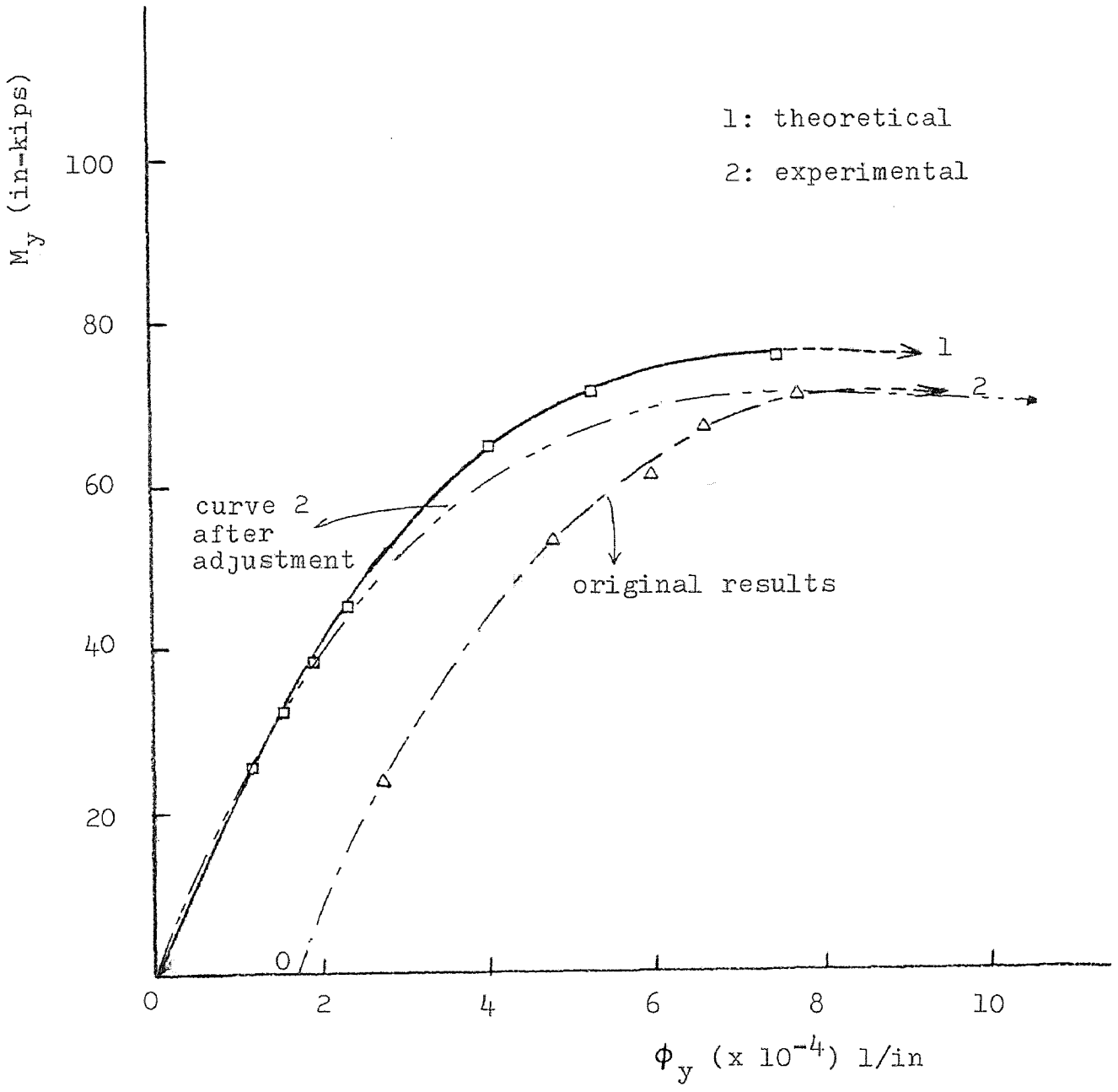

Fig. 2-4-4 MOMENT-CURVATURE DIAGRAM IN Y-DIRECTION

CHAPTER III

INTERACTION DIAGRAMS FOR L-SHAPED REINFORCED CONCRETE SHORT COLUMNS

3-1 INTRODUCTION

All these previous studies in section 2-1 have shown that Bresler's idea of failure surfaces and his proposed equations were the most convenient design methods for solving the problem of columns under biaxial bending and axial compression. Several tests indicated that both the reciprocal load equation (Eq. 2-1) and the load contour equation (Eq. 2-3) gave results that agree with experimental works. Most of the experiments done were based on short columns including both square and rectangular cross-sections. The load contour equation (Eq. 2-3) is easy to apply if the exponential, α, is known, but to find the value of α is a difficult problem because many parameters are involved. The reciprocal load equation is easier to apply but less research has been developed for it than that of the load contour method. In ACI Building Code it is required that for all compression members are subjected to bending about both principal axes, the moment about each axis must be amplified by a factor δ, computed from the corresponding conditions of restraint about the axis. But no experimental data are available in support of this

requirement.

However, no one has studied for L-shaped reinforced concrete columns by using these concepts. In this Chapter, an investigation of the behavior of L-shaped reinforced concrete column under biaxial bending and axial compression will be presented. The interaction diagrams and failure surface will be studied in details.

3-2 ANALYSIS

3-2-1 PROCEDURE FOR ANALYSIS

The cross-section of L-shaped reinforced concrete column used for analysis is shown as Fig. 2-4-1. Two different values of the maximum concrete compressive stress f_c' have been used which are 3500psi. and 5000psi., respectively. Five different inclined angle, α, are used in order to draw the interaction diagrams for moment M_x or M_y with respect to the compressive force P_n (where $\tan\alpha = e_y / e_x$). The interaction diagrams of uniaxial bending moment combined with the axial compression for both cases in X-direction and Y-direction must be found first (which are $\alpha = 90^\circ$ and $\alpha = 0^\circ$). Then choose three additional inclinations, α, to draw an interaction diagrams for M_x or M_y with axial compression. The cross-section has the same properties and data as in Chapter 2, except the maximum concrete compressive stress f_c' and the spacing of ties (S = 2 in. in this case). (refer to section 2-4-1)

3-2-2 NUMERICAL DATA

Five groups of inclination, α, for both cases are chosen. Each group includes five sets of eccentricity e_x and e_y. Then by using axis rotation as discussed in Chapter 2, e_x and e_y are transfered to e_u and e_v, which are shown as follows:

(i) $\alpha = 0^o$

(1) e_r = 1 in.: e_x = 1 in.; e_u = 0.891 in.
e_y = 0 in.; e_v = 0.454 in.

(2) e_r = 2 in.: e_x = 2 in.; e_u = 1.782 in.
e_y = 0 in.; e_v = 0.908 in.

(3) e_r = 3 in.: e_x = 3 in.; e_u = 2.763 in.
e_y = 0 in.; e_v = 1.362 in.

(4) e_r = 5 in.: e_x = 5 in.; e_u = 4.455 in.
e_y = 0 in.; e_v = 2.270 in.

(5) e_r = 10in.: e_x = 10in.; e_u = 8.910 in.
e_y = 0 in.; e_v = 4.540 in.

(ii) $\alpha = 30^o$

(1) e_r = 1 in.: e_x = 0.866 in.; e_u = 0.999 in.
e_y = 0.5 in.; e_v = 0.052 in.

(2) e_r = 2 in.: e_x = 1.732 in.; e_u = 1.997 in.
e_y = 1.0 in.; e_v = 0.105 in.

(3) e_r = 3 in.: e_x = 2.598 in.; e_u = 2.996 in.
e_y = 1.5 in.; e_v = 0.157 in.

(4) e_r = 5 in.: e_x = 4.330 in.; e_u = 4.993 in.
e_y = 2.500 in.; e_v = 0.262 in.

(5) e_r = 10in.: e_x = 8.660 in.; e_u = 9.986 in.
e_y = 5.000 in.; e_v = 0.523 in.

(iii) $\alpha = 45^\circ$

(1) e_r = 1 in.: e_x = 0.707 in.; e_u = 0.951 in.
e_y = 0.707 in.; e_v = 0.309 in.

(2) e_r = 2 in.: e_x = 1.414 in.; e_u = 1.902 in.
e_y = 1.414 in.; e_v = 0.618 in.

(3) e_r = 3 in.: e_x = 2.121 in.; e_u = 2.853 in.
e_y = 2.121 in.; e_v = 0.927 in.

(4) e_r = 5 in.: e_x = 3.536 in.; e_u = 4.756 in.
e_y = 3.536 in.; e_v = 1.545 in.

(5) e_r = 10in.: e_x = 7.071 in.; e_u = 9.510 in.
e_y = 7.071 in.; e_v = 3.090 in.

(iv) $\alpha = 60^\circ$

(1) e_r = 1 in.: e_x = 0.5 in.; e_u = 0.839 in.
e_y = 0.866 in.; e_v = 0.545 in.

(2) e_r = 2 in.: e_x = 1.0 in.; e_u = 1.677 in.
e_y = 1.732 in.; e_v = 1.089 in.

(3) e_r = 3 in.: e_x = 1.5 in.; e_u = 2.516 in.
e_y = 2.598 in.; e_v = 1.634 in.

(4) e_r = 5 in.: e_x = 2.5 in.; e_u = 4.193 in.
e_y = 4.33 in.; e_v = 2.723 in.

(5) e_r = 10in.: e_x = 5.0 in.; e_u = 8.387 in.
e_y = 8.66 in.; e_v = 5.446 in.

(v) $\alpha = 90^o$

(1) e_r = 1 in.: e_x = 0 in.; e_u = 0.454 in.
e_y = 1.0 in.; e_v = 0.891 in.

(2) e_r = 2 in.: e_x = 0 in.; e_u = 0.908 in.
e_y = 2.0 in.; e_v = 1.782 in.

(3) e_r = 3 in.: e_x = 0 in.; e_u = 1.362 in.
e_y = 3.0 in.; e_v = 2.673 in.

(4) e_r = 5 in.: e_x = 0 in.; e_u = 2.270 in.
e_y = 5.0 in.; e_v = 4.455 in.

(5) e_r = 10in.: e_x = 0 in.; e_u = 4.540 in.
e_y = 10.0 in.; e_v = 8.910 in.

From these investigations, the ultimate strength of this section for both cases can be found. By computer output, these results M_u and M_v are corresponding to the principal axes. For practical purpose, M_u and M_v are transferred to M_x and M_y which are corresponding to the centriodal axes by using the concept of transformation matrix mentioned in Chapter 2. After the transformation, the results are plotted on the interaction diagrams and these interaction curves for combined bending moment and axial compression are shown in Fig. 3-2-1 through Fig. 3-2-20.

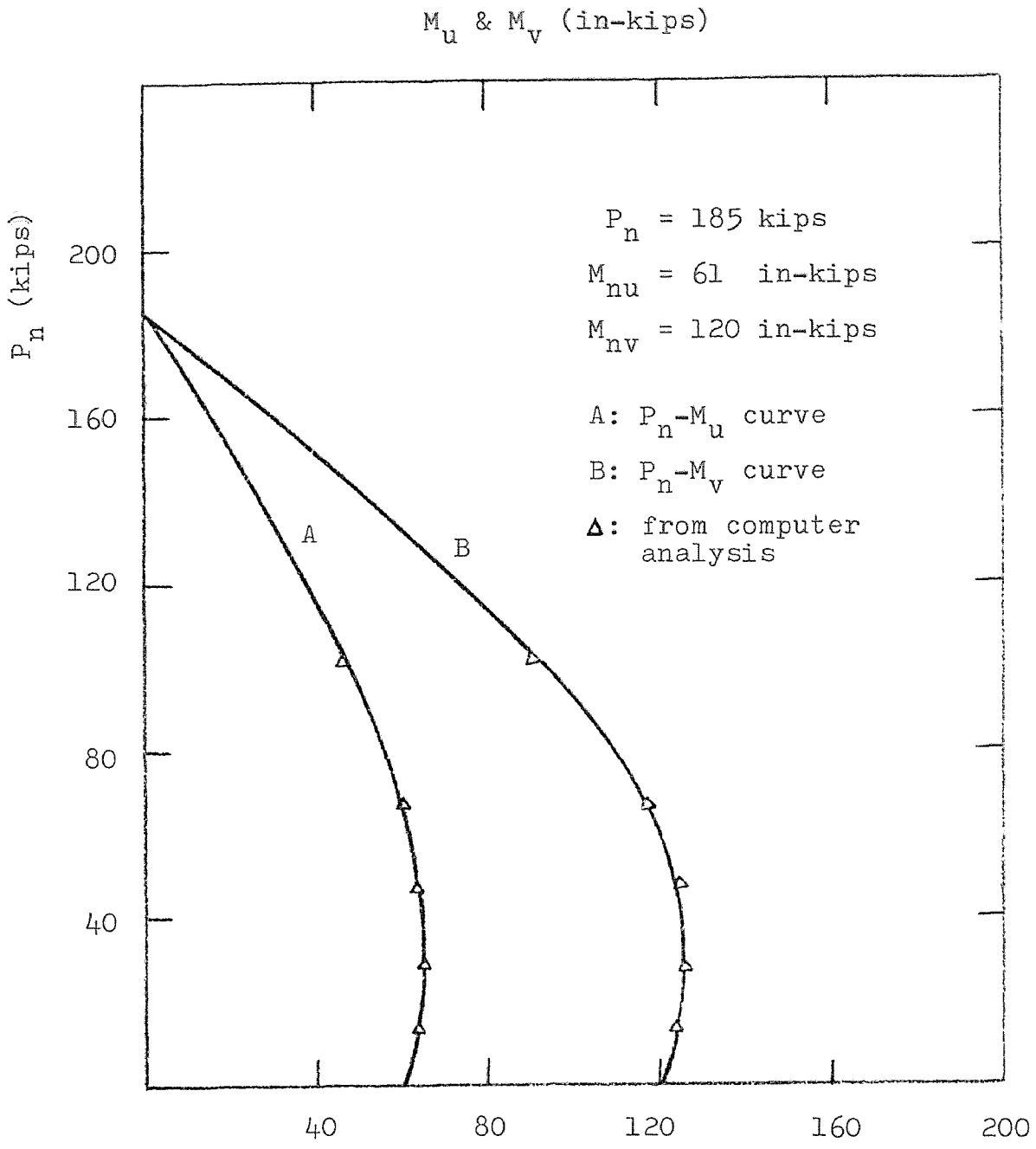

Fig. 3-2-1 INTERACTION DIAGRAM CORRESPONDING TO PRINCIPAL AXES (f_c' = 3500 psi, $\alpha = 0^o$)

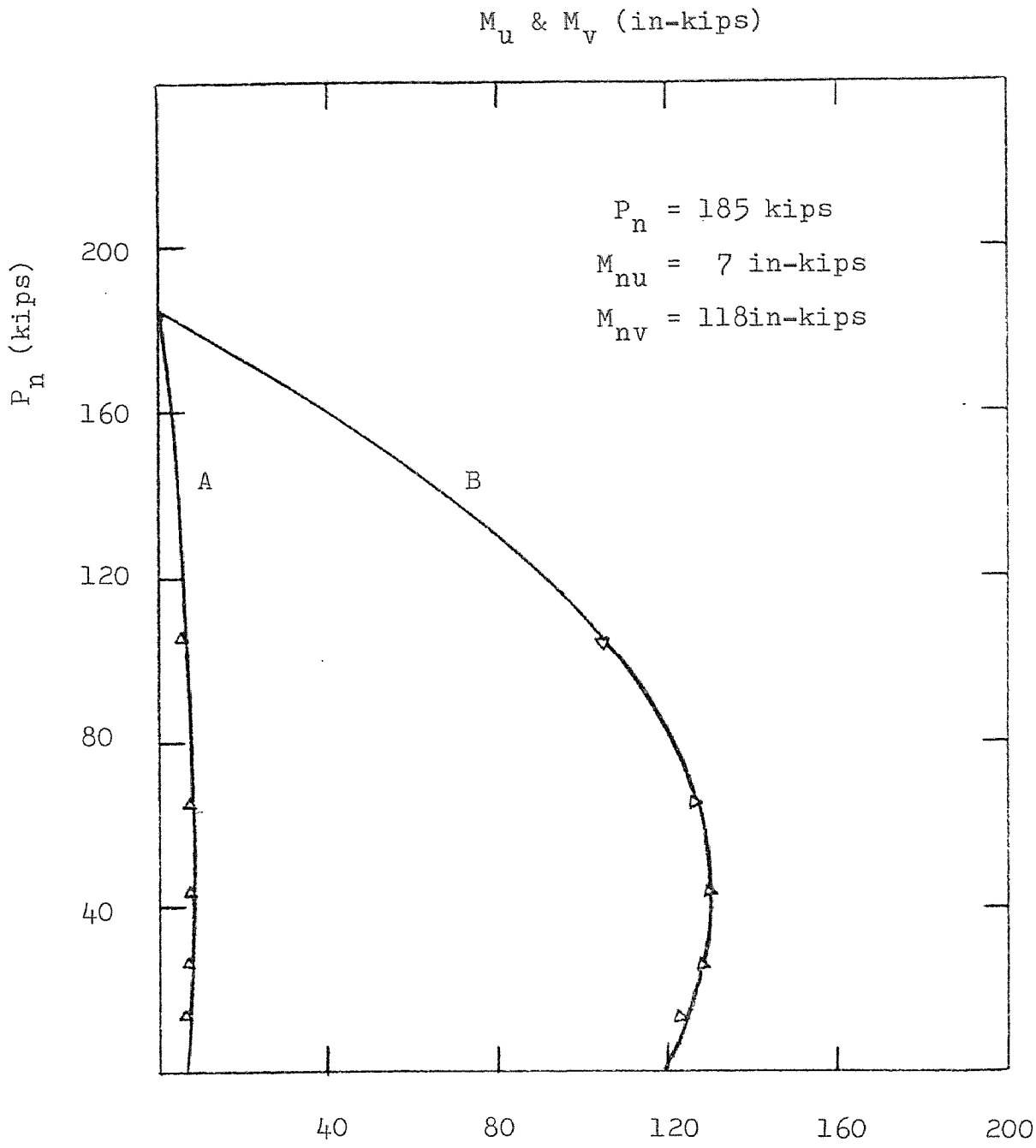

Fig. 3-2-2 INTERACTION DIAGRAM CORRESPONDING TO PRINCIPAL AXES (f_c' = 3500 psi, $\alpha = 30^\circ$)

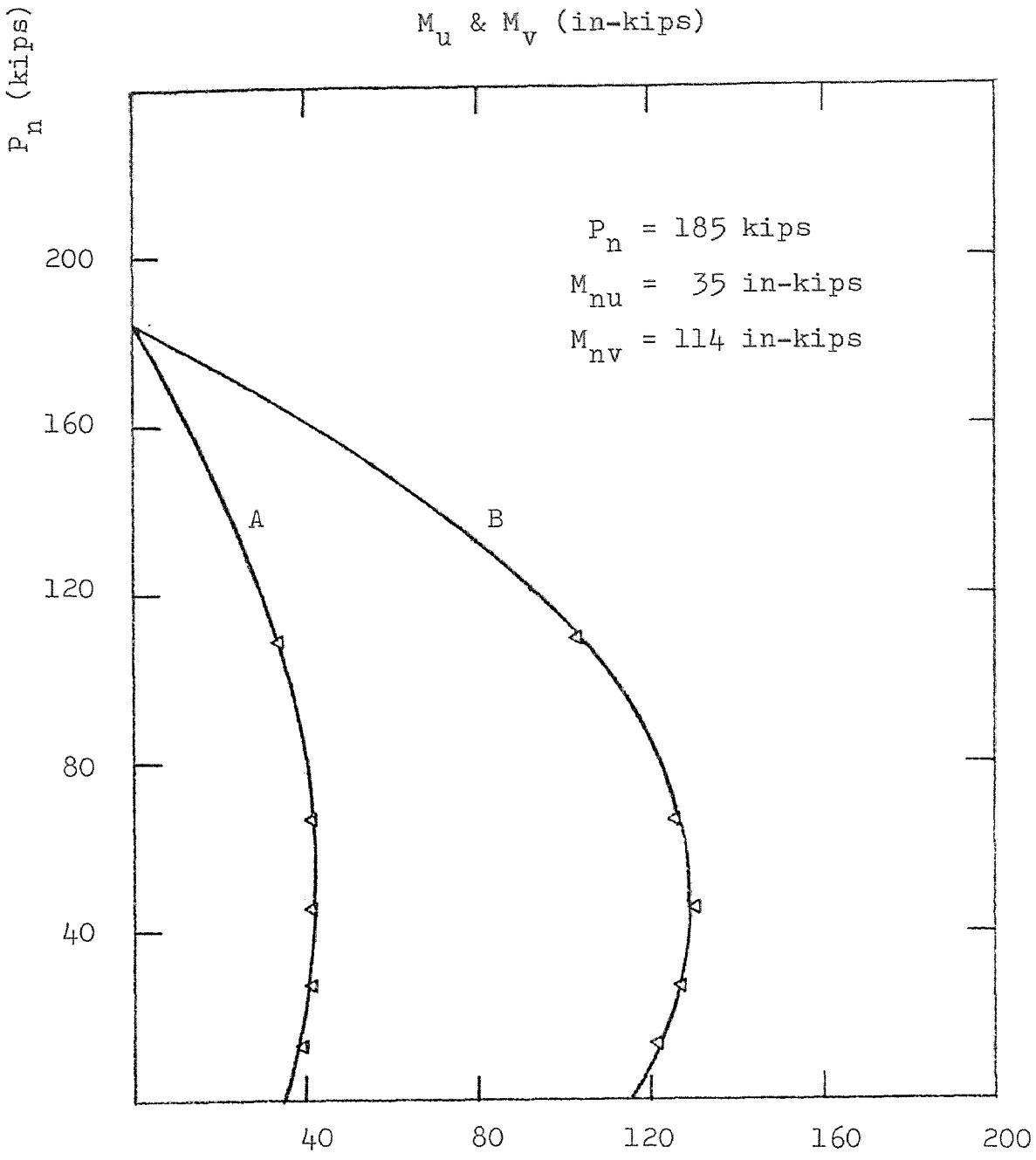

Fig. 3-2-3 INTERACTION DIAGRAM CORRESPONDING TO PRINCIPAL AXES (f_c' = 3500 psi, $\alpha = 45^\circ$)

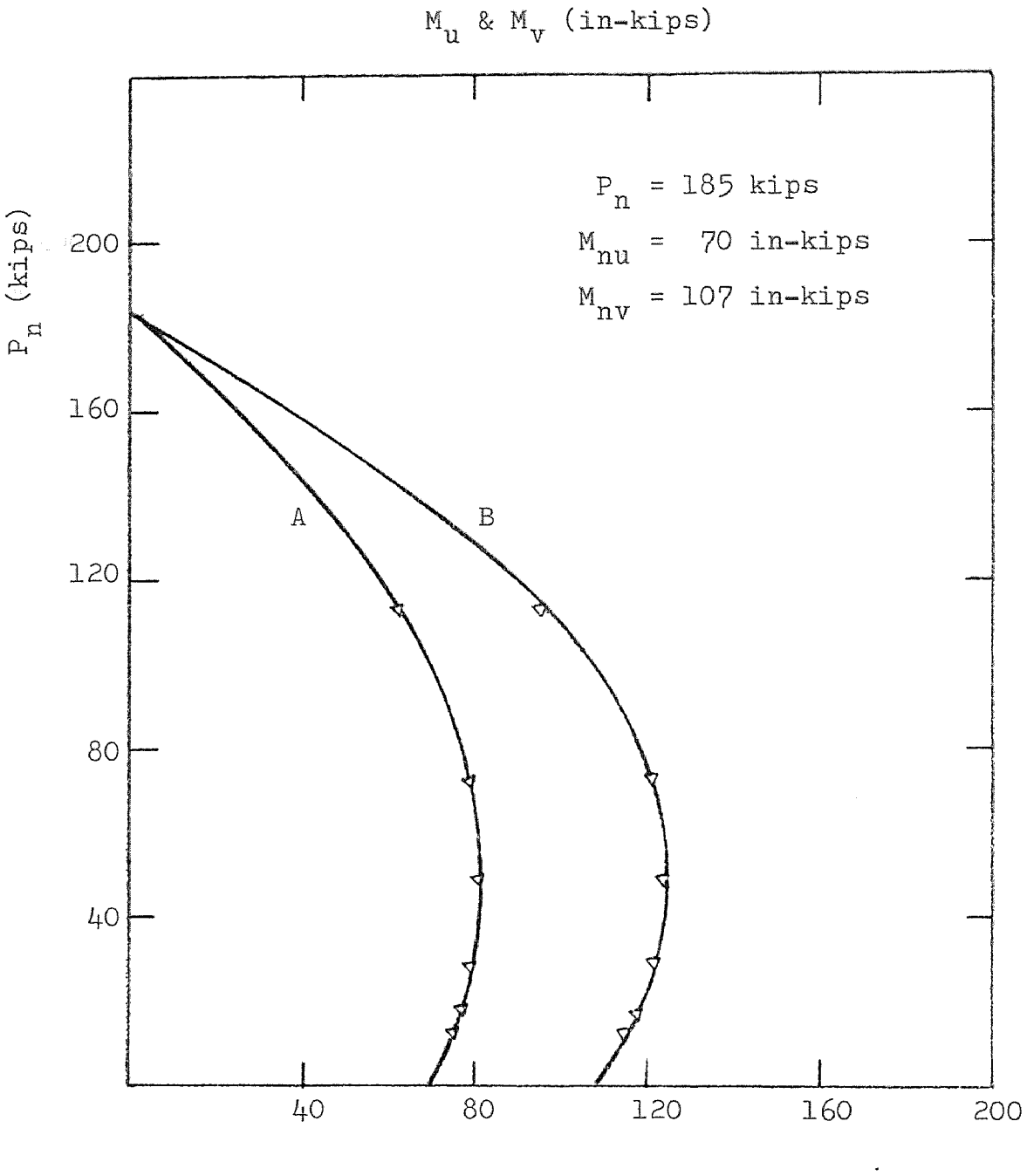

Fig. 3-2-4 INTERACTION DIAGRAM CORRESPONDING TO PRINCIPAL AXES (f_c' = 3500 psi, $\alpha = 60^\circ$)

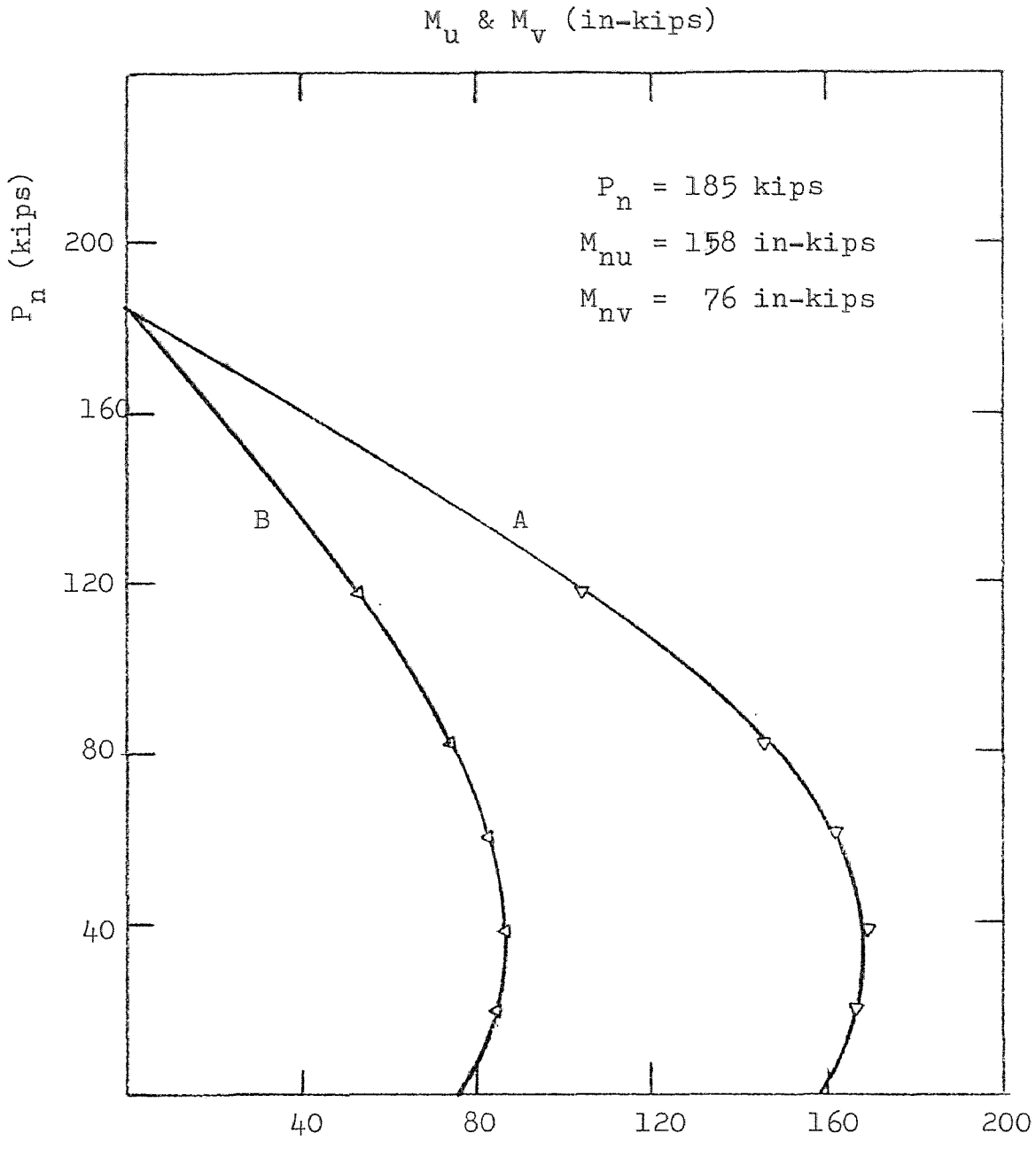

Fig. 3-2-5 INTERACTION DIAGRAM CORRESPONDING TO PRINCIPAL AXES (f_c' = 3500 psi, $\alpha = 90^\circ$)

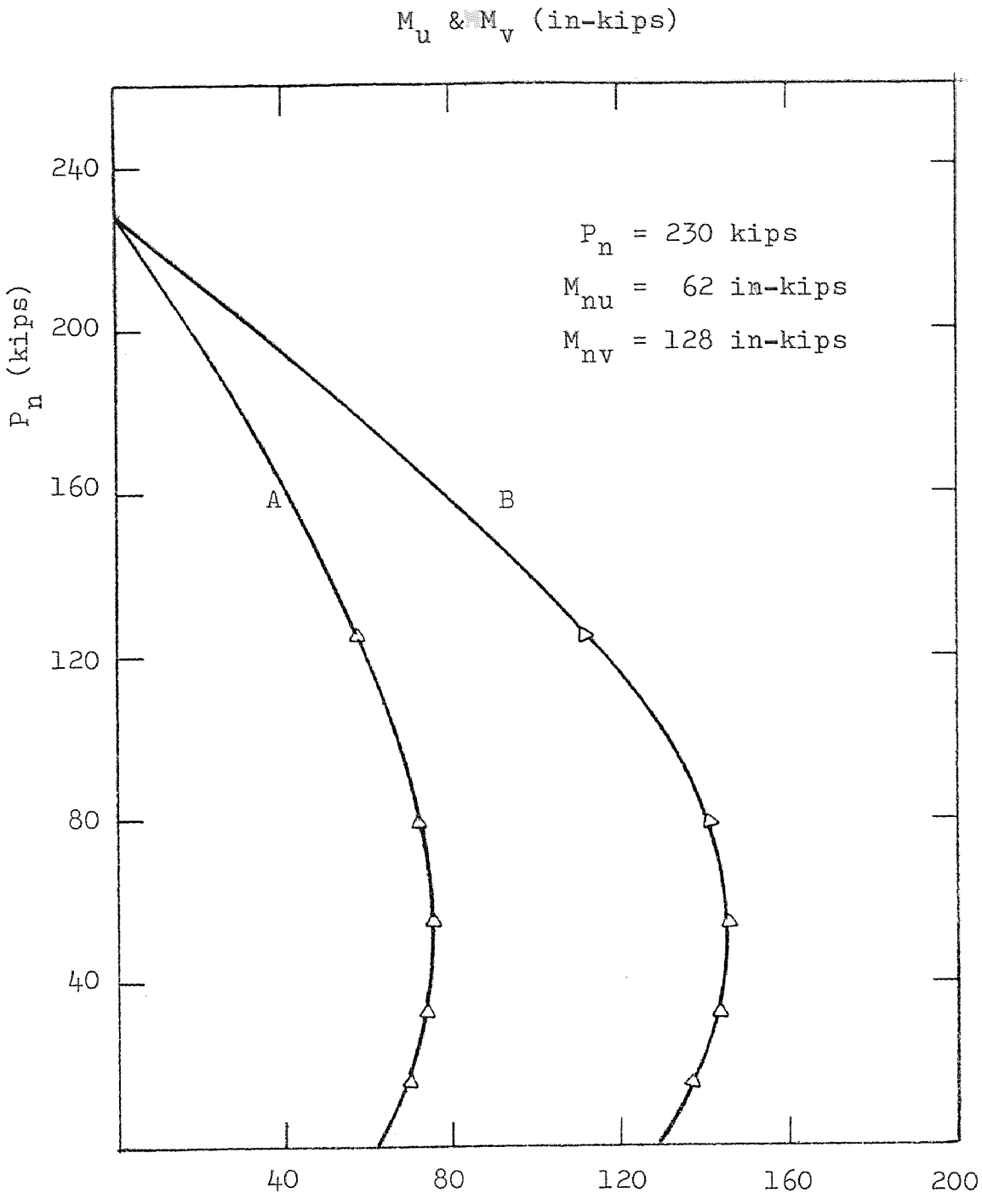

Fig. 3-2-6 INTERACTION DIAGRAM CORRESPONDING TO PRINCIPAL AXES (f_c' = 5000 psi, $\alpha = 0^\circ$)

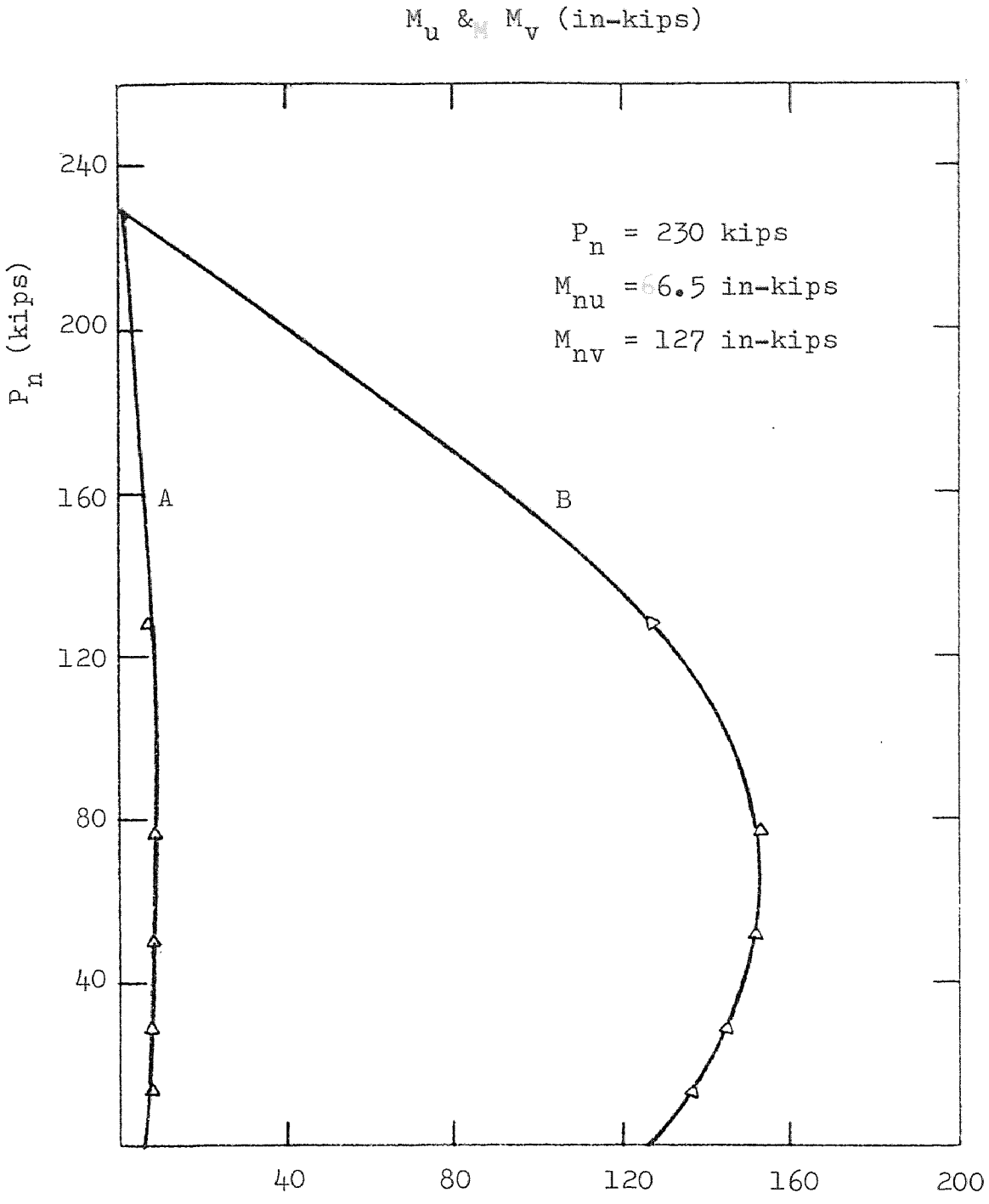

Fig. 3-2-7 INTERACTION DIAGRAM CORRESPONDING TO PRINCIPAL AXES (f_c' =5000 psi, $\alpha = 30^o$)

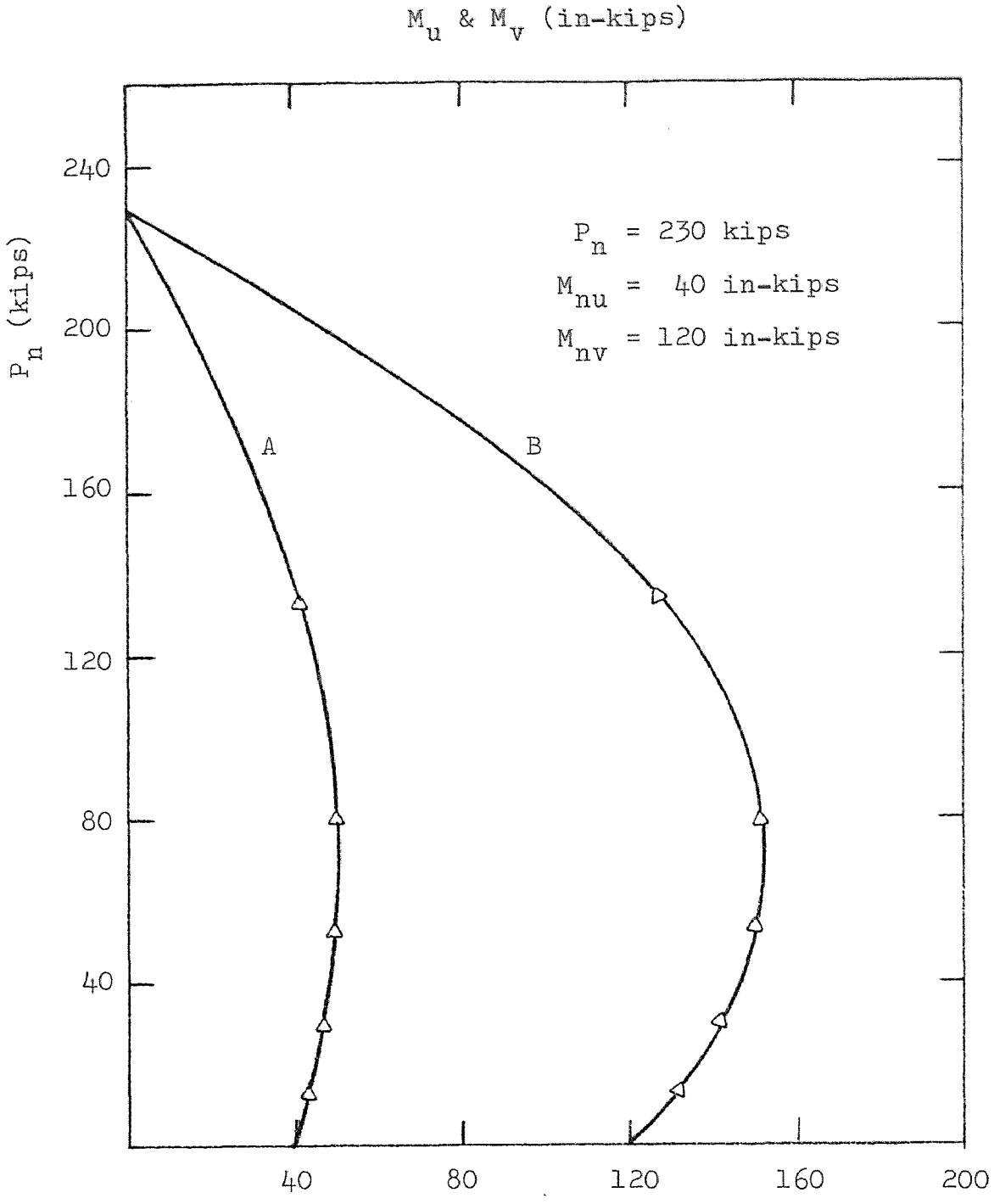

Fig. 3-2-8 INTERACTION DIAGRAM CORRESPONDING TO PRINCIPAL AXES (f_c' = 5000psi, $\alpha = 45^\circ$)

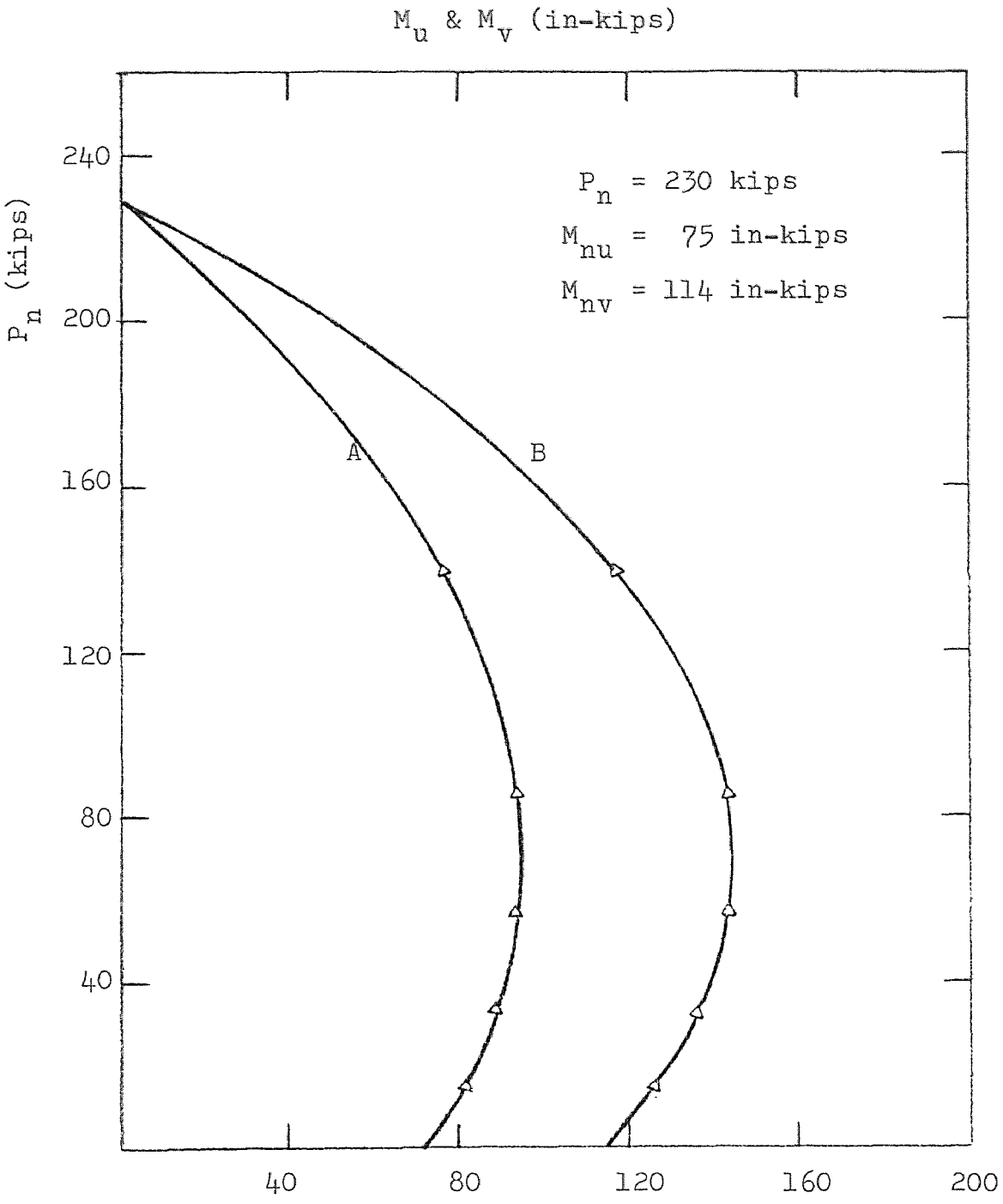

Fig. 3-2-9 INTERACTION DIAGRAM CORRESPONDING TO PRINCIPAL AXES (f_c' = 5000 psi, $\alpha = 60^o$)

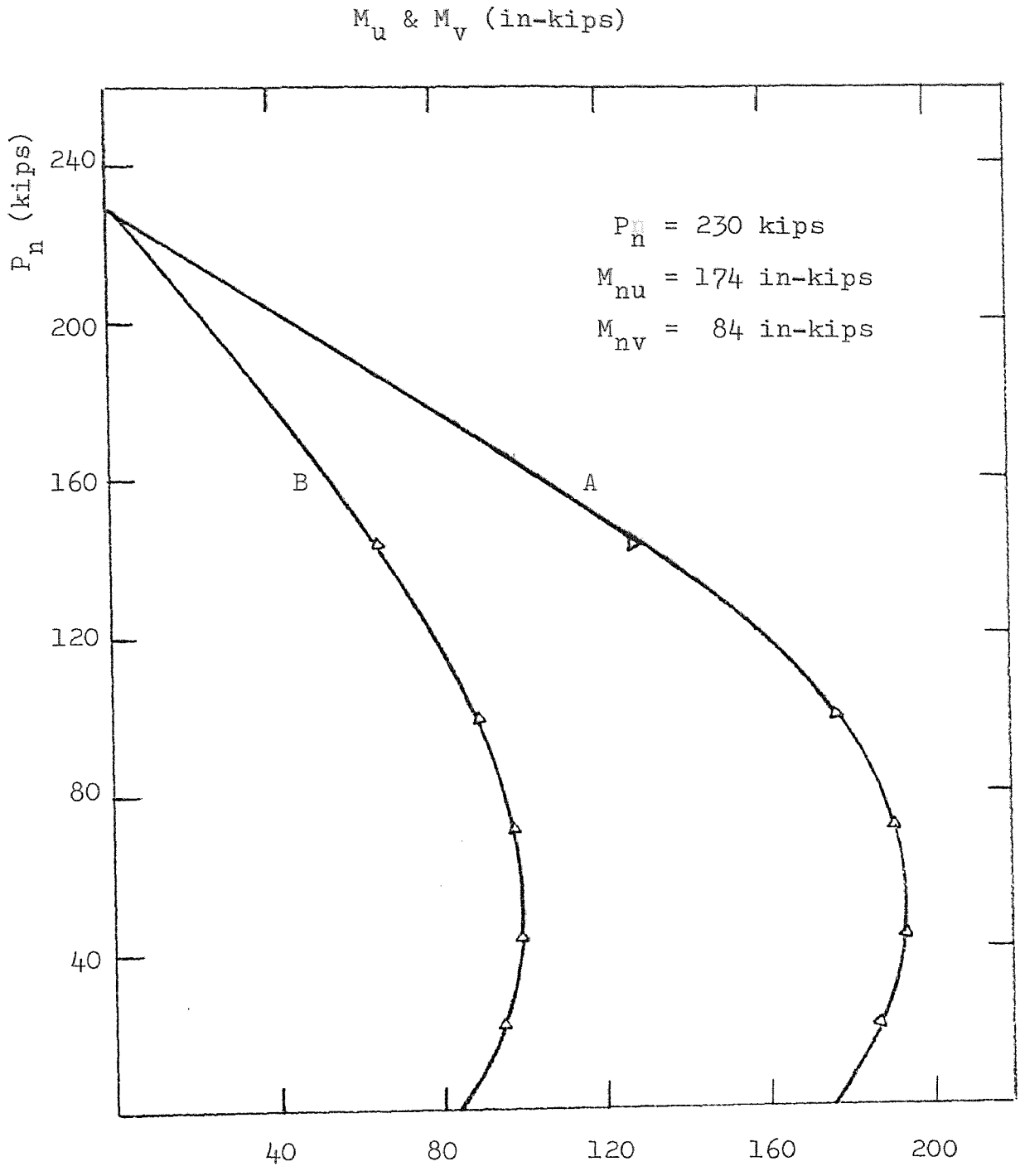

Fig. 3-2-10 INTERACTION DIAGRAM CORRESPONDING TO PRINCIPAL AXES (f_c' = 5000 psi, $\alpha = 90^o$)

3-3 ANALYSIS RESULTS OF INTERACTION DIAGRAMS FOR COLUMN UNDER COMBINED BENDING MOMENT AND AXIAL COMPRESSION

Those interaction diagrams as shown in 3-2 are based on the analysis of results of the computer program which includes uniaxial or biaxial bending combined with the axial compression condition. The ultimate axial compression are 185 Kips for f_c' = 3500 psi. and 230 kips for f_c' = 5000 psi. resulting from the extrapolating the interaction curve to the compression axis. This result is the same as total steel area multiplied by the yielding strength of reinforcement (f_y = 51800 psi.) plus the net concrete area (A_c) multiplied by the maximum concrete compressive stress (f_c').(e.g. $P_n = A_c f_c' + A_s f_y$) The concrete stress f_c' was used without the usual reduction factor 0.85 for strength calculation.

Fig. 3-2-1 through Fig. 3-2-10 are the interaction curves corresponding to the principal axes U-axis and V-axis. Curve A and curve B are obtained from the failure compression combined with ultimate moments about U-axis and V-axis, respectively. Fig. 3-2-11 through Fig. 3-2-20 are the interaction curves corresponding to the centroidal axes:X-axis and Y-axis. Curve C and curve D are obtained from the failure compression combined with

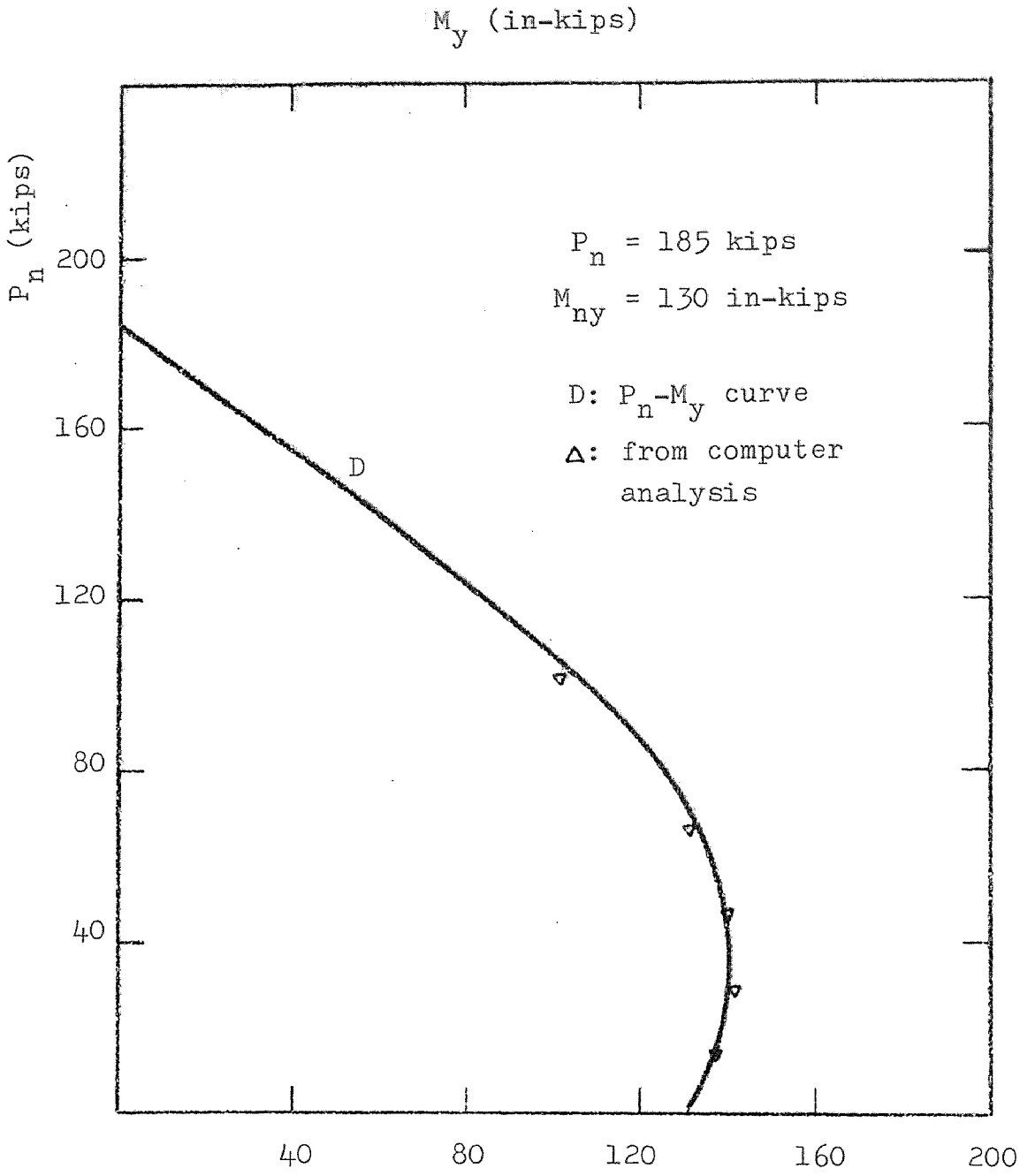

Fig. 3-2-11 INTERACTION DIAGRAM CORRESPONDING TO CENTROIDAL AXES (f_c' = 3500 psi, $\alpha = 0^o$)

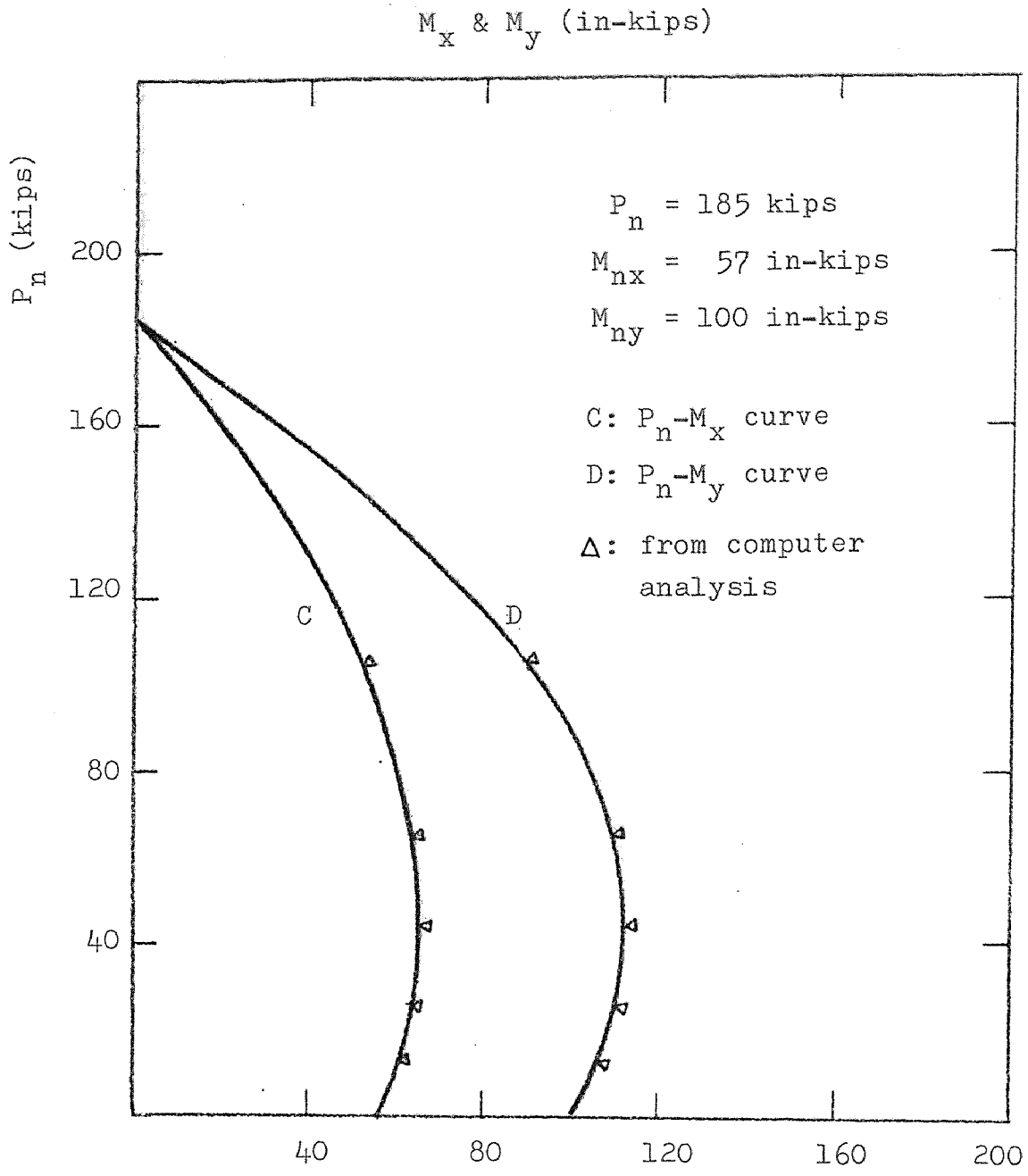

Fig. 3-2-12 INTERACTION DIAGRAM CORRESPONDING TO CENTROIDAL AXES (f_c' = 3500 psi, $\alpha = 30^\circ$)

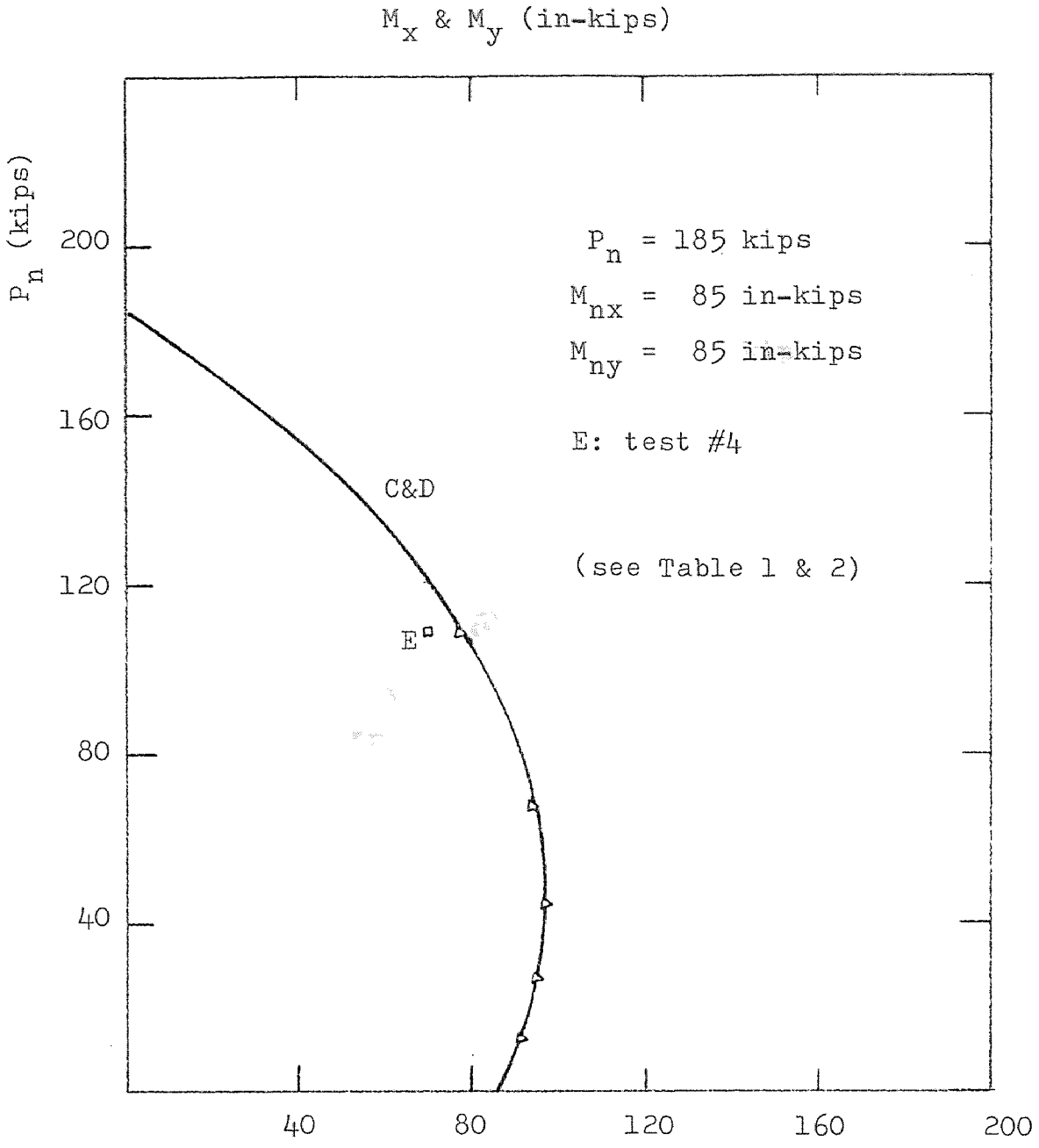

Fig. 3-2-13 INTERACTION DIAGRAM CORRESPONDING TO CENTROIDAL AXES (f_c' = 3500 psi, $\alpha = 45^o$)

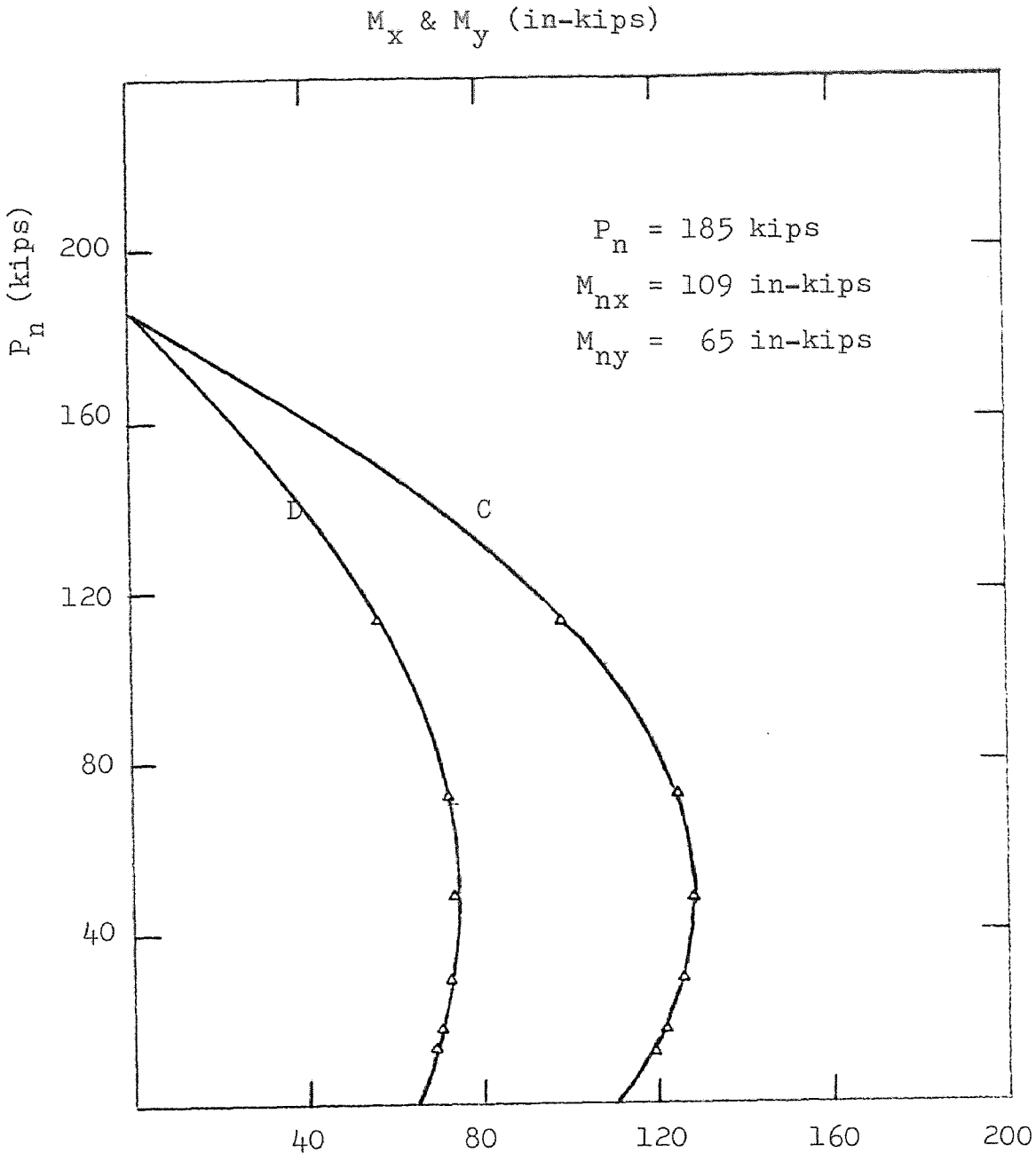

Fig. 3-2-14 INTERACTION DIAGRAM CORRESPONDING TO CENTROIDAL AXES (f_c' = 3500 psi, $\alpha = 60^\circ$)

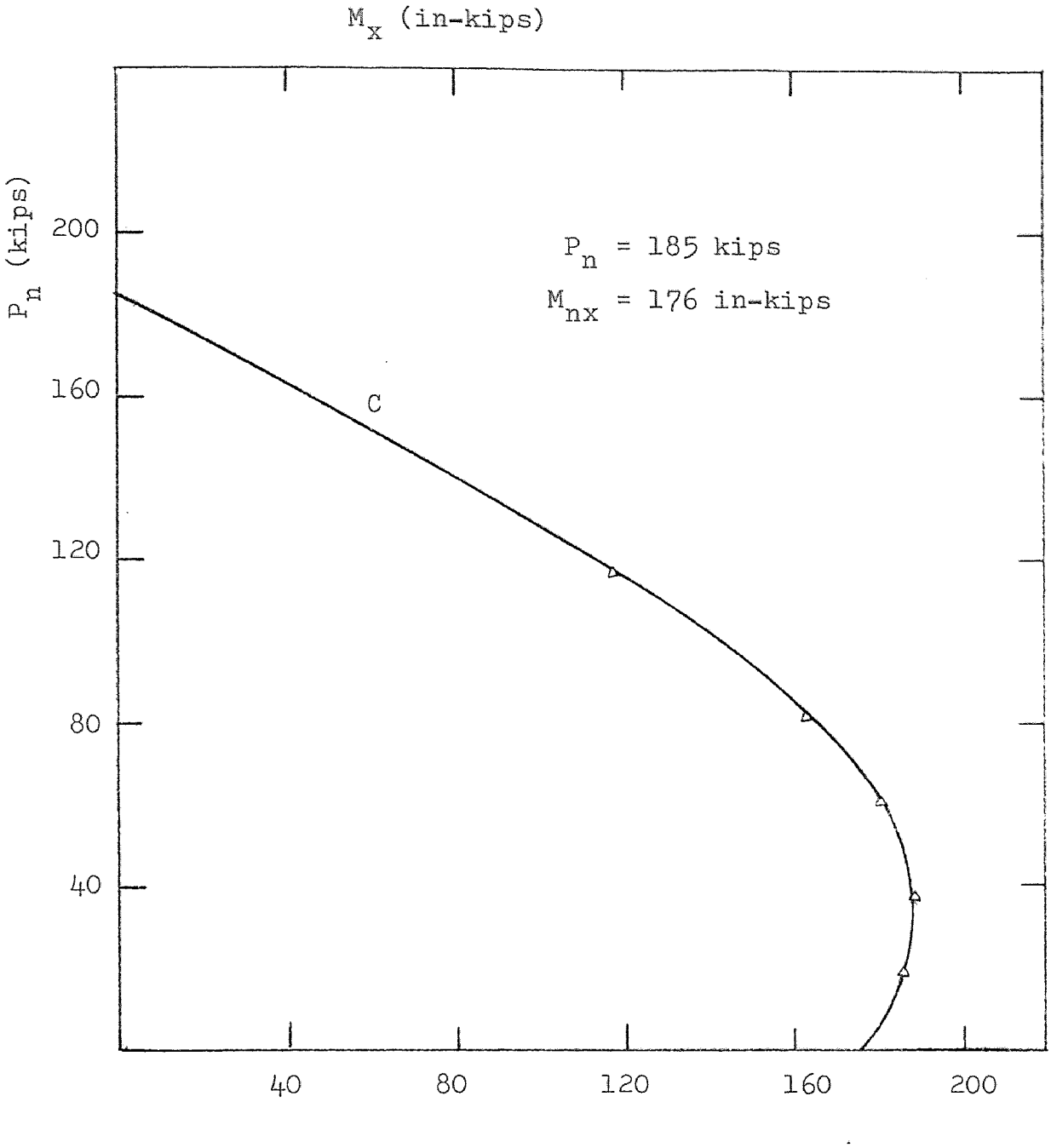

Fig. 3-2-15 INTERACTION DIAGRAM CORRESPODING TO CENTROIDAL AXES (f_c' = 3500 psi, $\alpha = 90^o$)

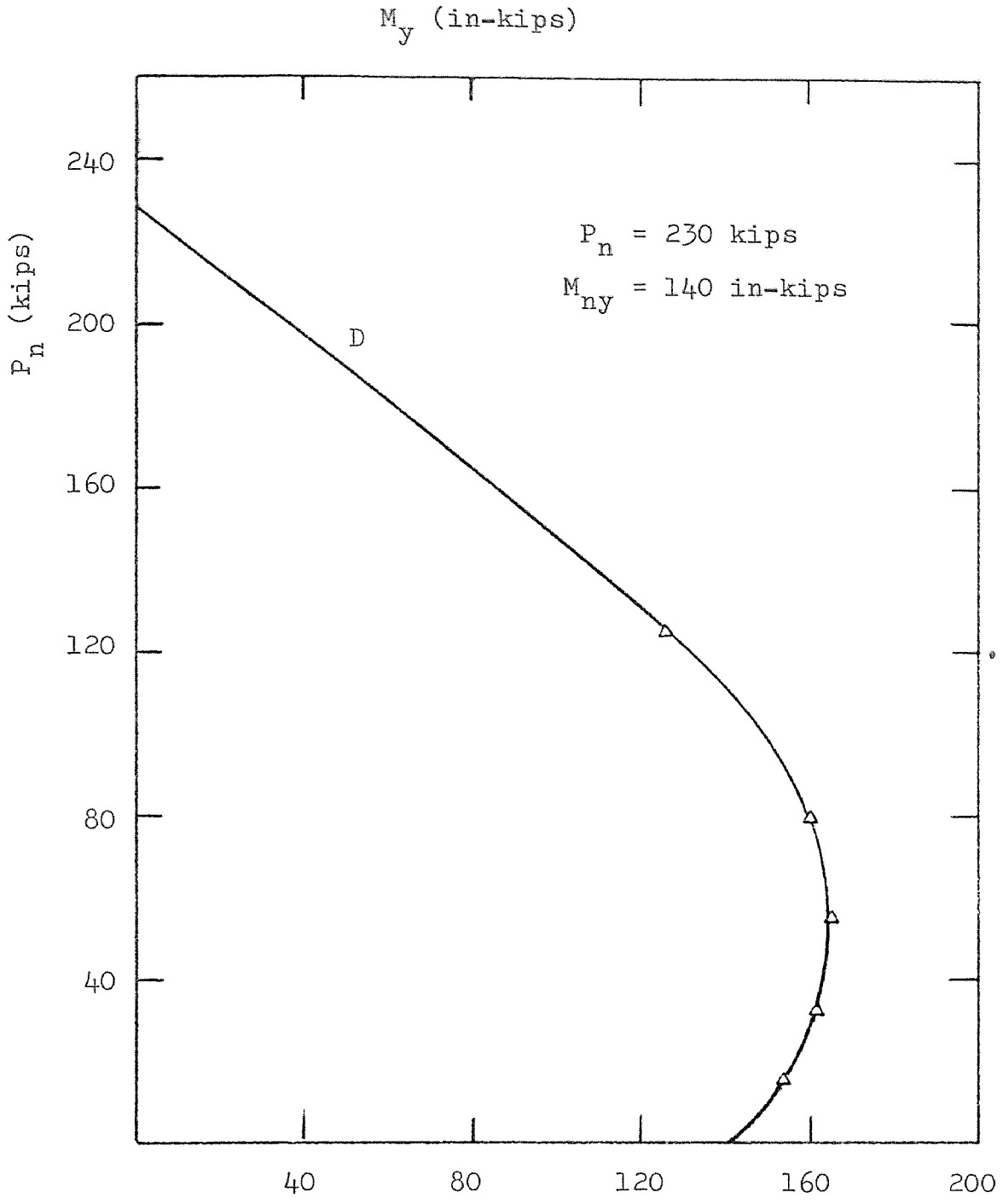

Fig. 3-2-16 INTERACTION DIAGRAM CORRESPONDING TO CENTROIDAL AXES (f_c' = 5000 psi, $\alpha = 0^o$)

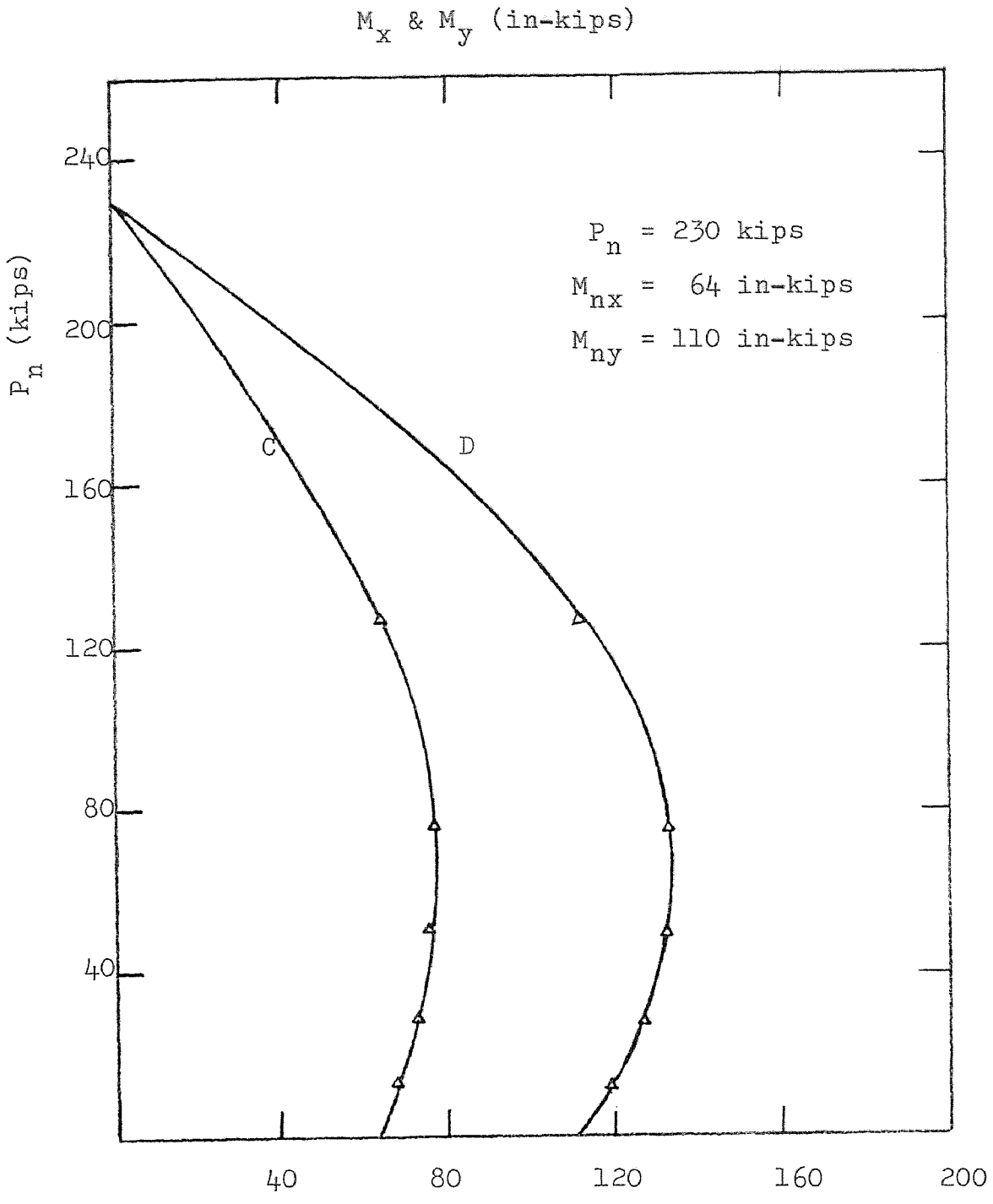

Fig. 3-2-17 INTERACTION DIAGRAM CORRESPONDING TO CENTROIDAL AXES (f_c' = 5000 psi, α = 30°)

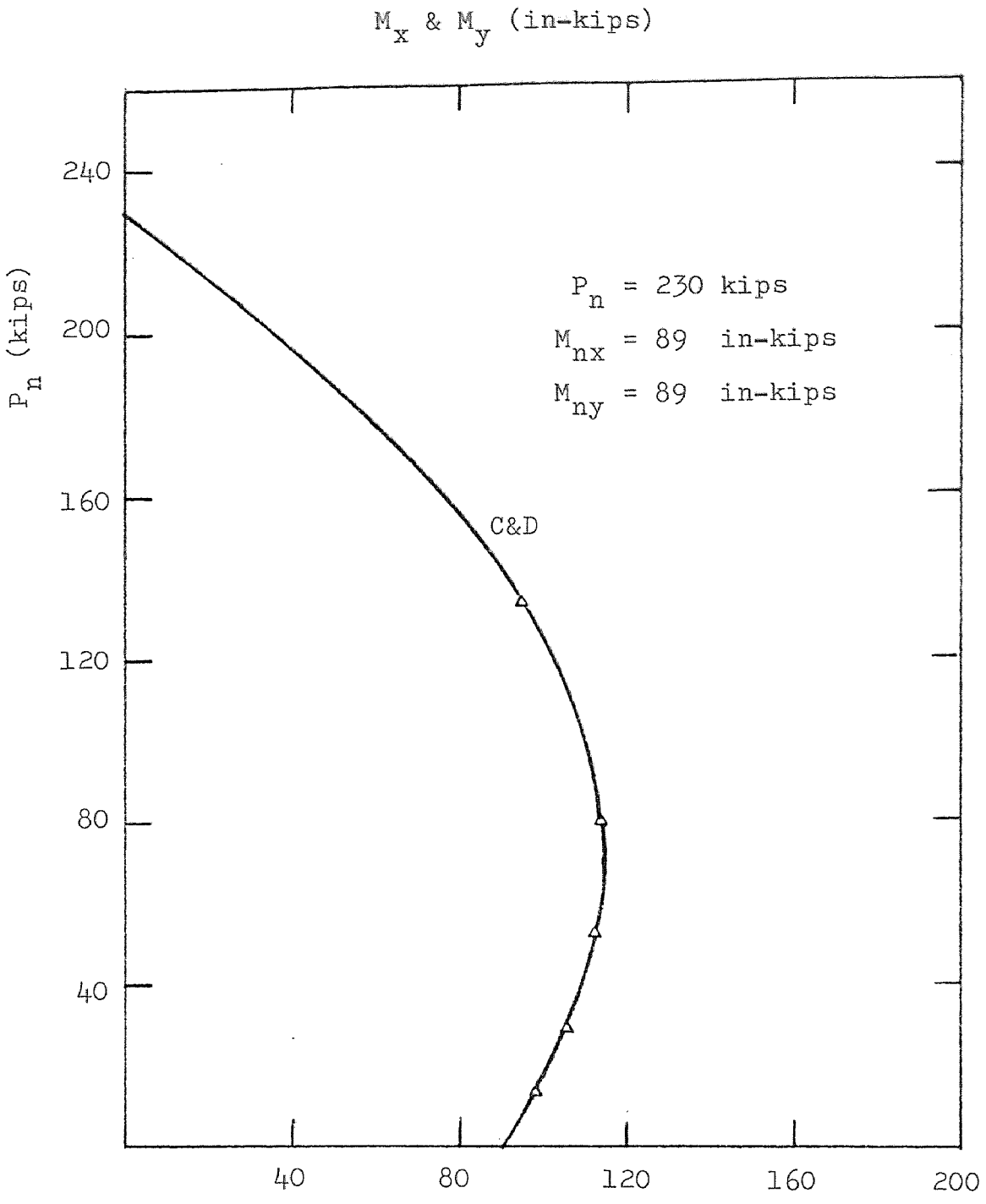

Fig. 3-2-18 INTERACTION DIAGRAM CORRESPONDING TO CENTROIDAL AXES (f_c' = 5000 psi, $\alpha = 45^o$)

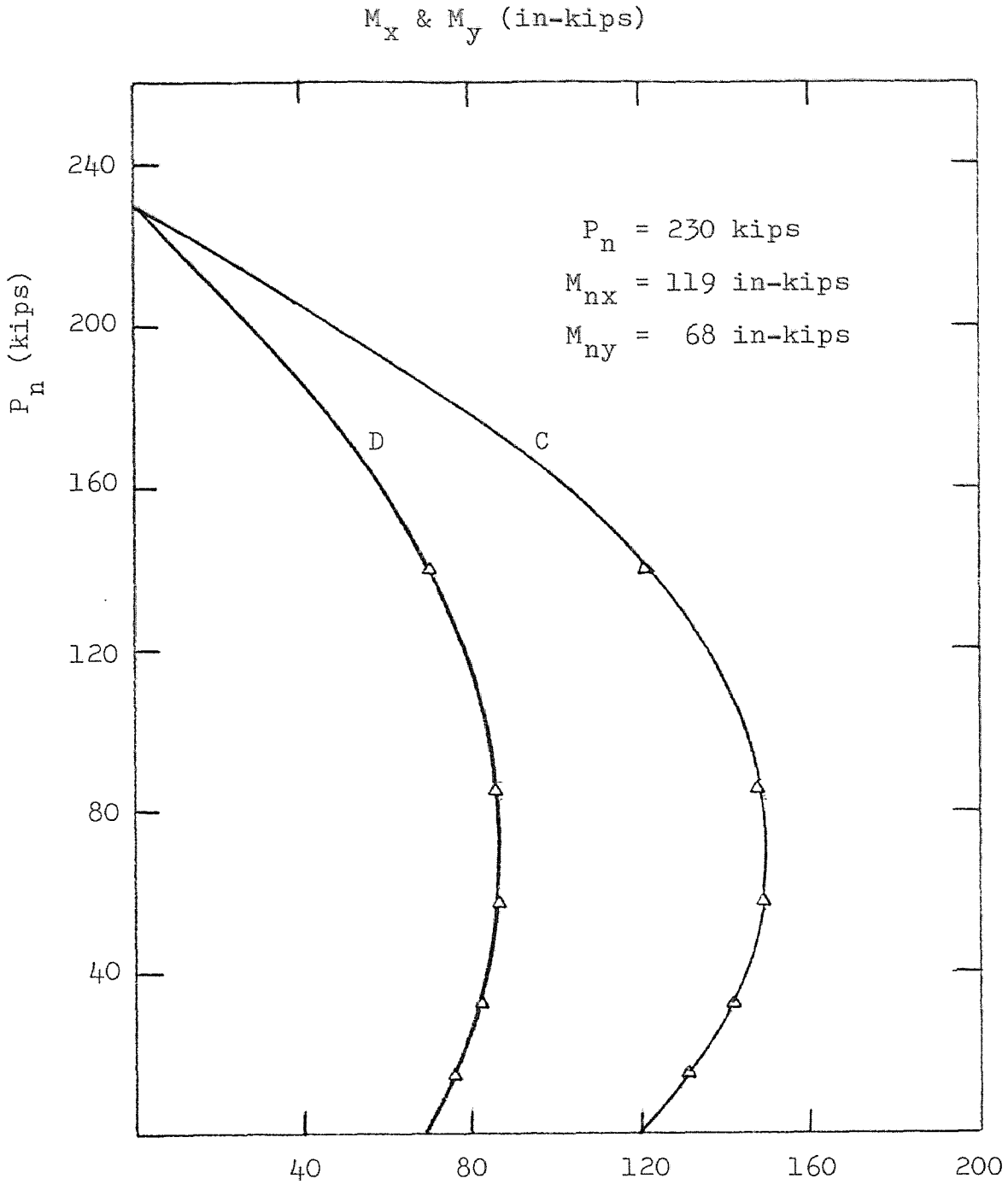

Fig. 3-2-19 INTERACTION DIAGRAM CORRESPONDING TO CENTROIDAL AXES (f_c' = 5000 psi, $\alpha = 60^o$)

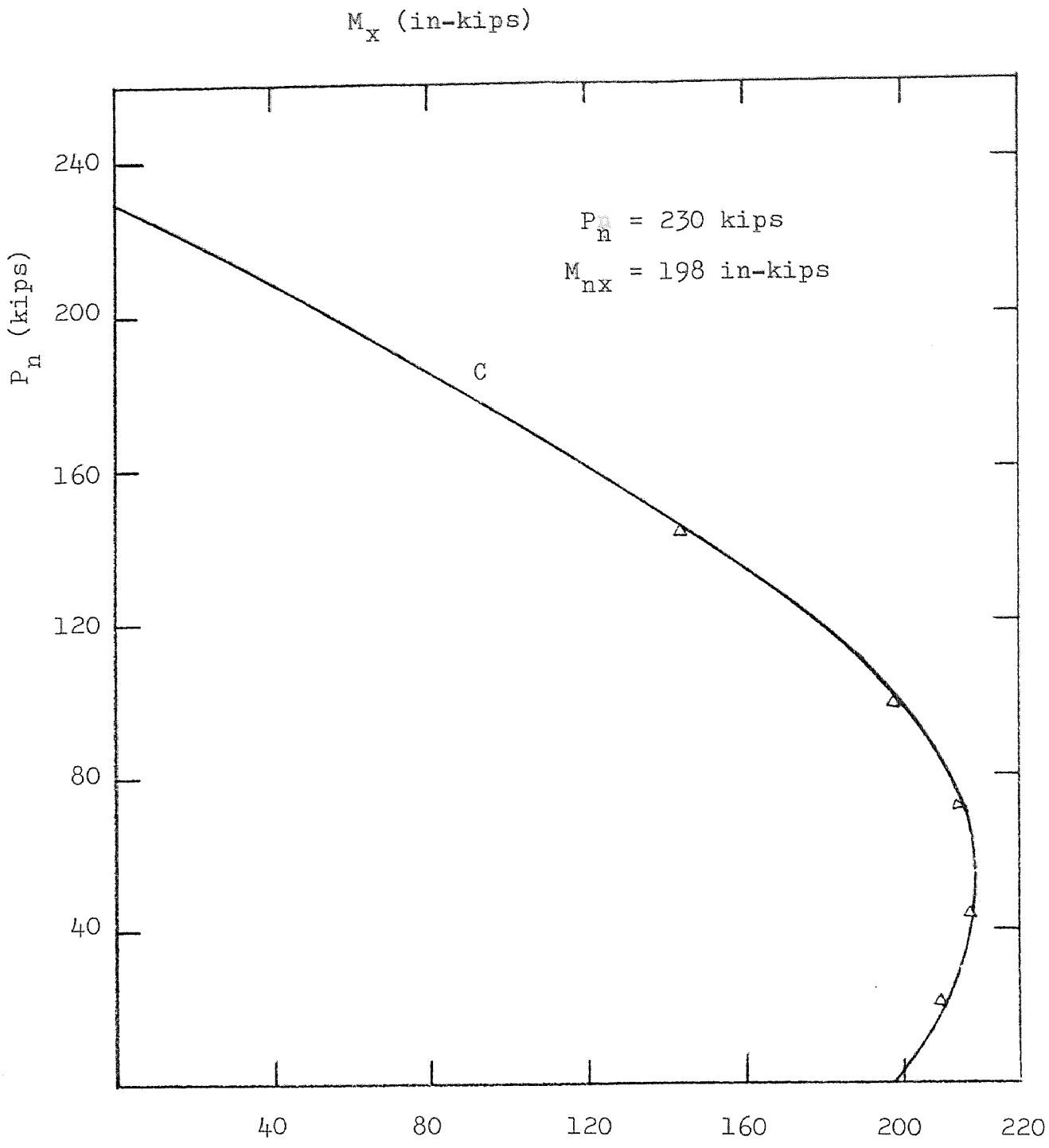

Fig. 3-2-20 INTERACTION DIAGRAM CORRESPONDING TO CENTROIDAL AXES (f_c' = 5000 psi, $\alpha = 90^\circ$)

ultimate moments about X-axis and Y-axis, respectively.

In Fig. 3-2-13, Fig. 3-2-18 the interaction curves in compression combined with moments about X-axis and Y-axis are the same, since the inclination $\alpha = 45^{o}$. All these interaction curves pass through the point in pure compression (185 Kips for f_c' = 3500psi. and 230Kips for f_c' = 5000psi.). Besides, all these curves are smooth in shape, and are similar to those curves for rectangular or square cross-section of the reinforced concrete columns. Point E of Fig. 3-2-13 is the experimental result. For example, point E, this specimen has ties spacing S = 3in., $e_x = e_y$ = 0.643in., with failure compression P_n = 109Kips and $M_x = M_y$ = 70.7ft-Kips.. The difference is about 7% as comapred with the theoretical values P_n = 116.5Kips. The reasons for this difference are: (1) different spacing of ties (S = 3in. for experiment and S = 2in. for computer analysis) (2) Mid-height deflections are not included in computing the bending moments for experiment. However, both cases are close enough.

3-4 LOAD CONTOURS OF L-SHAPED MEMBER SUBJECT TO COMBINED LOADING

Referring to Fig. 2-1-3, the failure surfaces for rectangular cross-section columns under combined axial

compression and biaxial bending moments have been studied for several years. The writer uses the same load contour concept and develops the failure surface for L-shaped reinforced concrete column. The load contour diagrams shown in Fig. 3-4-1 are based on the interaction diagrams of the L-shaped column with f_c' = 3500psi.. Constant loads of P_n = 40Kips, 80Kips, 120Kips and 160Kips have been selected. The load contour diagrams of the second section as shown in Fig. 3-4-2, are based on the interaction diagrams shown in Fig. 3-2-16 through Fig. 3-2-20. Unfortunately, the load contour diagrams are not circular arc. A nondimensional load contour shown in Fig. 3-4-3 is used to study the deviation for L-shaped cross-section reinforced concrete columns.

All load contours at the constant load are parabolic curves and the interaction diagrams for P_n - M_{nx} and P_n - M_{ny} are also parabolic curves. However, there are different interaction diagrams and load contours for the different irregular sections. This needs more further investigation.

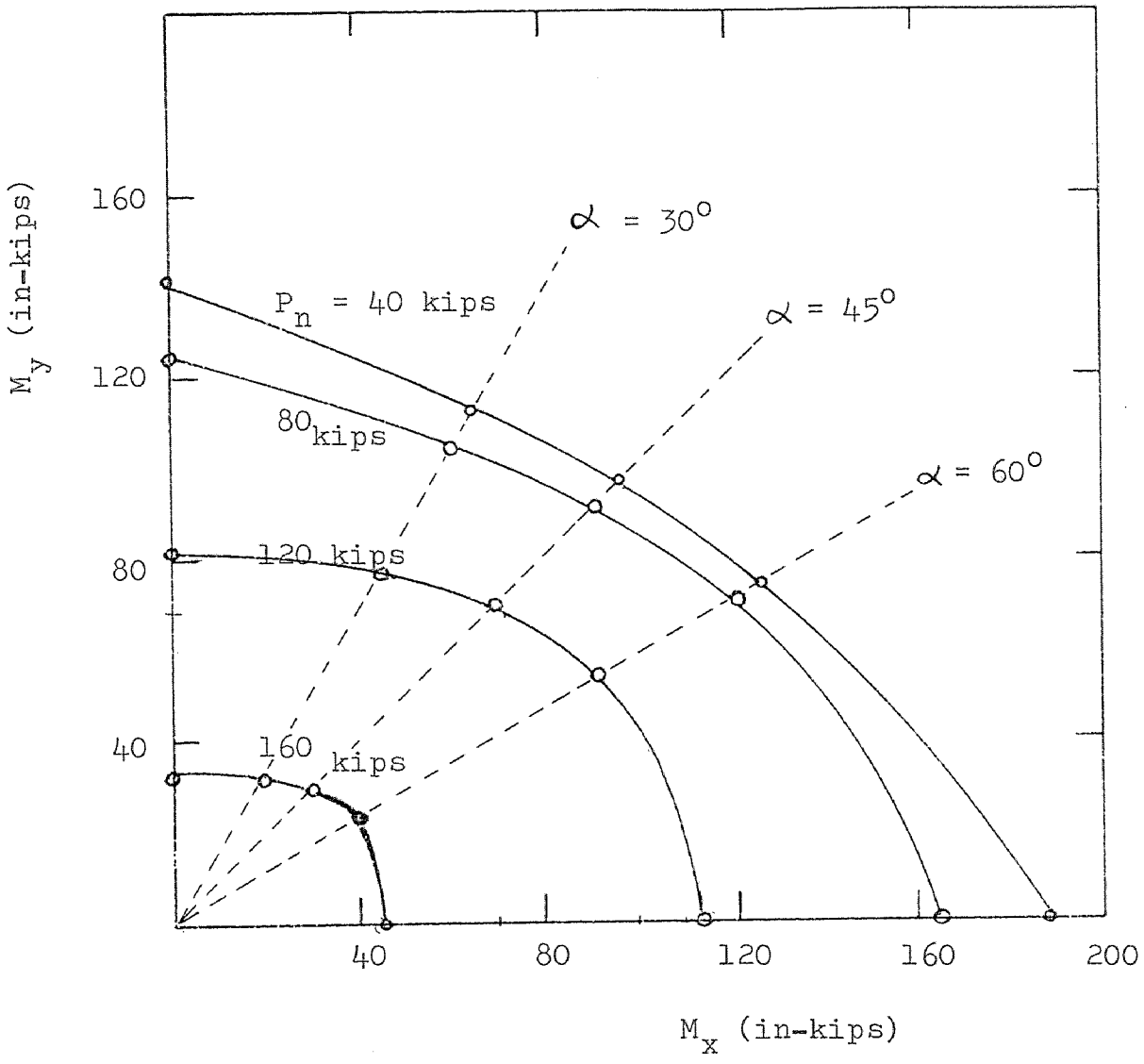

Fig. 3-4-1 LOAD CONTOURS FOR f_c' = 3500 psi

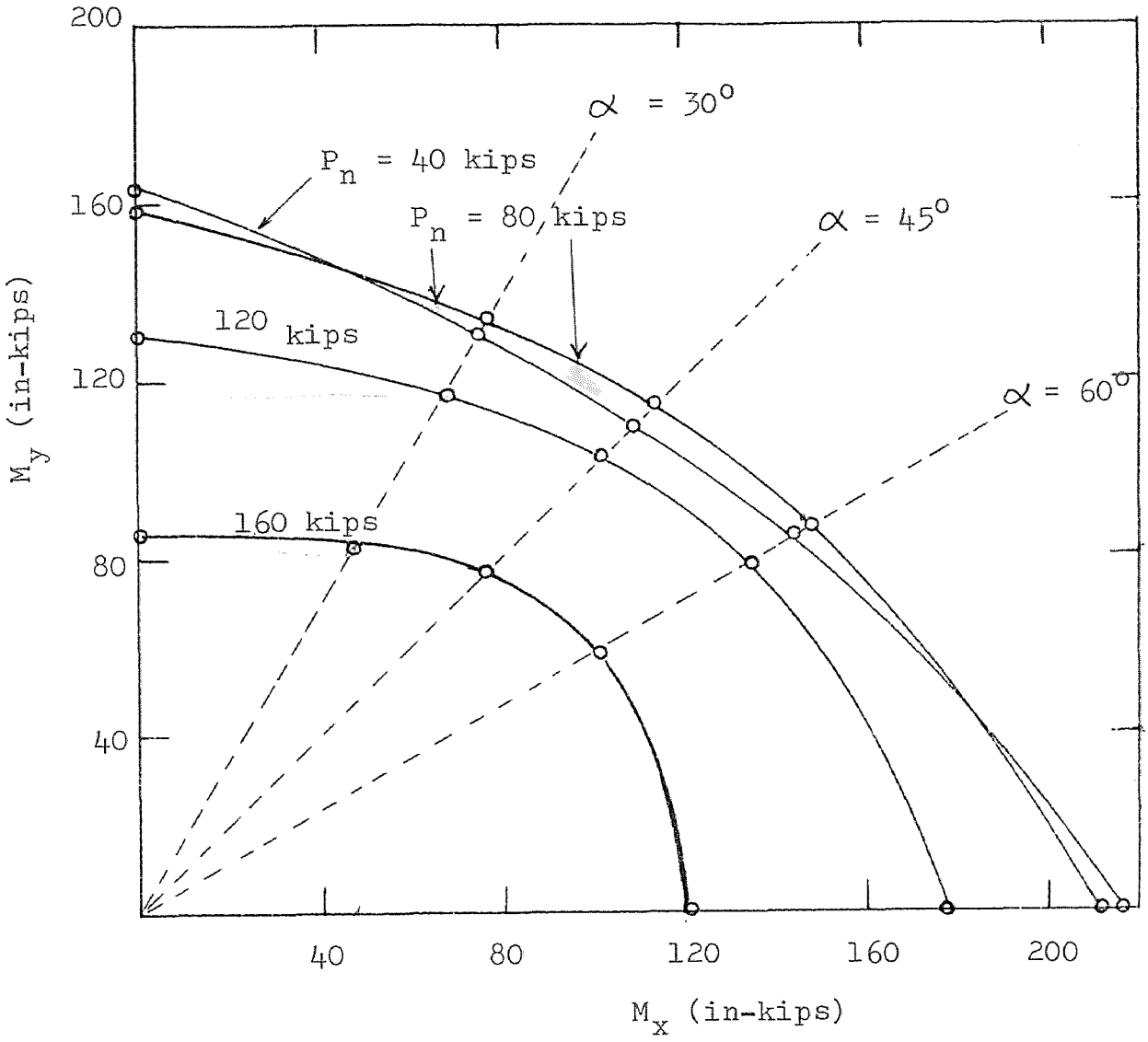

Fig. 3-4-2 LOAD CONTOURS FOR f_c' = 5000 psi

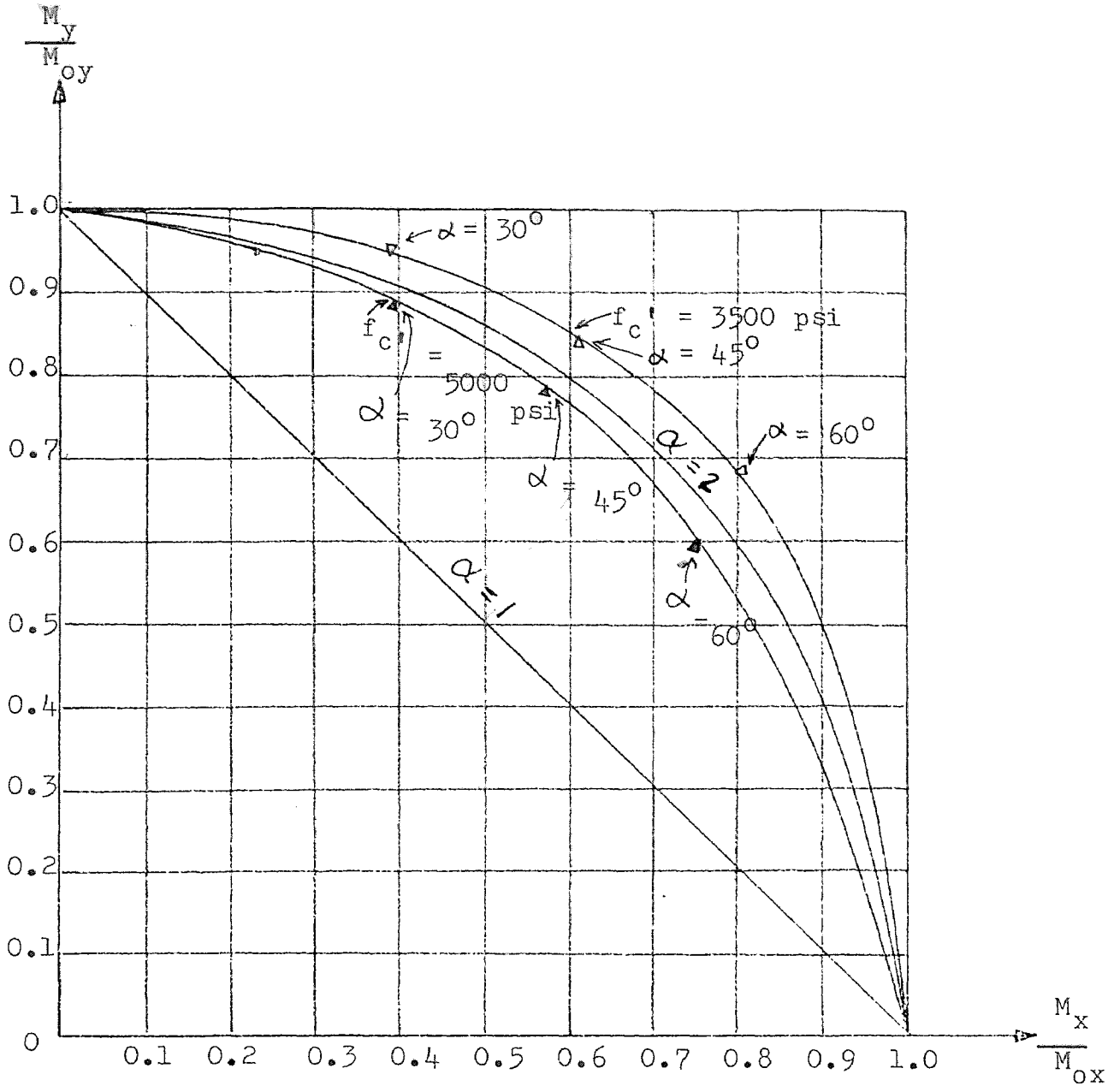

Fig. 3-4-3 NONDIMENSIONAL LOAD CONTOURS FOR BOTH f_c' = 3500 psi AND f_c' = 5000 psi (WHEN P_n = 120 kips)

CHAPTER IV

THREE-DIMENSIONAL FAILURE SURFACE FOR L-SHAPED REINFORCED CONCRETE COLUMNS

4-1 TEST PROGRAM

In chapter 3, the interaction diagrams and load contours at the constant loads for L-shaped reinforced concrete columns under combined loading have been developed from the computer output. In this chapter, the writer would like to develop the theoretical three-dimensional failure surface. Furthermore, those theoretical results will be compared with the experimental tests by the others graduate students at the New Jersey Institute of Technology (26, 27).

Some L-shaped reinforced concrete short columns were tested under biaxial bending moments and axial compresion. The parameter studied is the eccentricity of the applied load. The specimens were divided into two groups. The first group was tested under monotonic loading while the second group was tested under cyclic loading. All these specimens have the same cross-section which is shown in Fig. 2-4-1. The reinforcement for all these specimens are consists of grade #3 bars as the longitudinal bar and that for column ties consists of

1/4 in. diameter plain steel wire ($As'' = 0.025$ in.^{2}). The stress-strain curves of both concrete and steel are the same as shown in Fig. 2-3-2 and Fig. 2-3-3. Other details of these specimens such as tie spacing S, eccentricities of applied load e_x, e_y and maximum concrete compressive stress f_c' are different. All these details and test results are shown in Table 2.

4-2 FAILURE SURFACE FOR L-SHAPED REINFORCED CONCRETE COLUMNS

Referring to chapter 2, the failure surfaces for symmetrical section reinforced concrete columns under combined bending moments and axial compression have been studied for several years. The writer uses the same load contour concept and develops the failure surface for L-shaped reinforced concrete columns under combined bending moments and axial compression. As discussed in chapter 3, the load contour diagrams at the constant loads for L-shaped members have been developed as shown in Fig. 3-4-1 and 3-4-2. Four constant loads of P_n = 40Kips, 80Kips, 120Kips and 160Kips have been selected. According to these studies, the failure surfaces for both f_c' = 3500psi and f_c' = 5000psi can be easy obtained as shown in Fig. 4-2-1 and Fig. 4-2-2. These results are similar with Marin's failure surfaces (see reference 7). In order to examine the validity of

TABLE 2: DETAILS OF SPECIMEN AND TEST RESULTS

ITEM	GROUP 1 MONOTONIC LOADING			GROUP 2 CYCLIC LOADING				
Specimen No.	#3	#4	#5	#6	#7	#8	#9	#10
Avg. f_c' (psi)	3776	3756	3726	3478	3510	3703	3868	3882
Ties spacing S (in.)	3	3	2	2	4	3	3	4
e_x (in.)	1.75	0.643	1.393	0.643	0.643	-0.857	0.643	1.393
e_y (in.)	0.25	0.643	-0.357	0.643	0.643	-1.295	0.643	-0.357
P_n (Kips.)	46.4	109	63.0	92.8	82.5	36.1	93	72.3
M_{nx} (in-Kips)	11.6*	70*	-22.5*	59.7*	53*	-46.7*	59.8*	-25.8*
M_{ny} (in-Kips)	81.2*	70*	87.8*	59.7*	53*	-30.9*	59.8*	100.7*
No. of Cycles	—	—	—	2	3	1	2	2

* Mid-height deflections are not included in computing the bending moment (Ref. 26, 27)

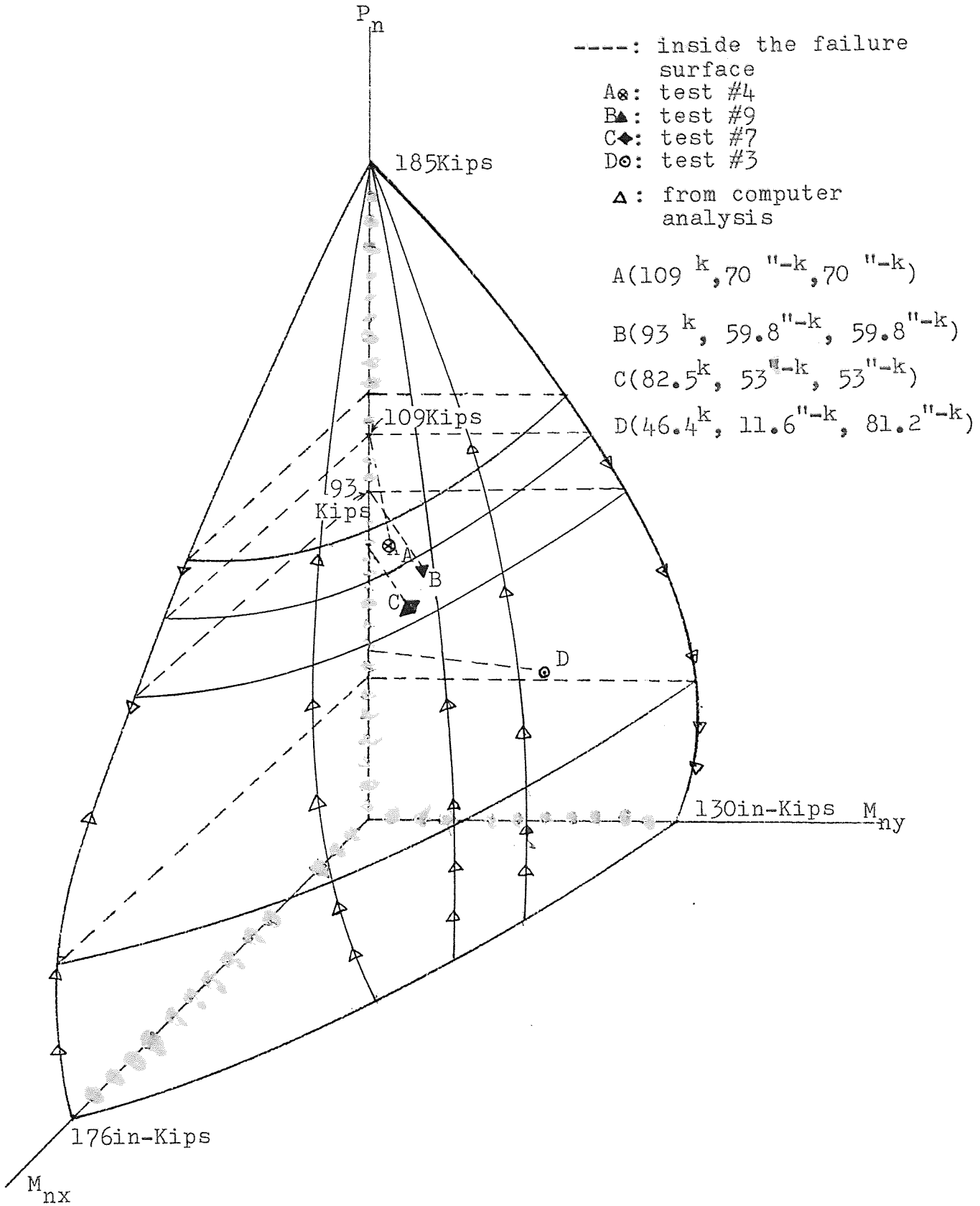

Fig. 4-2-1 FAILURE SURFACE FOR f_c' = 3500 psi

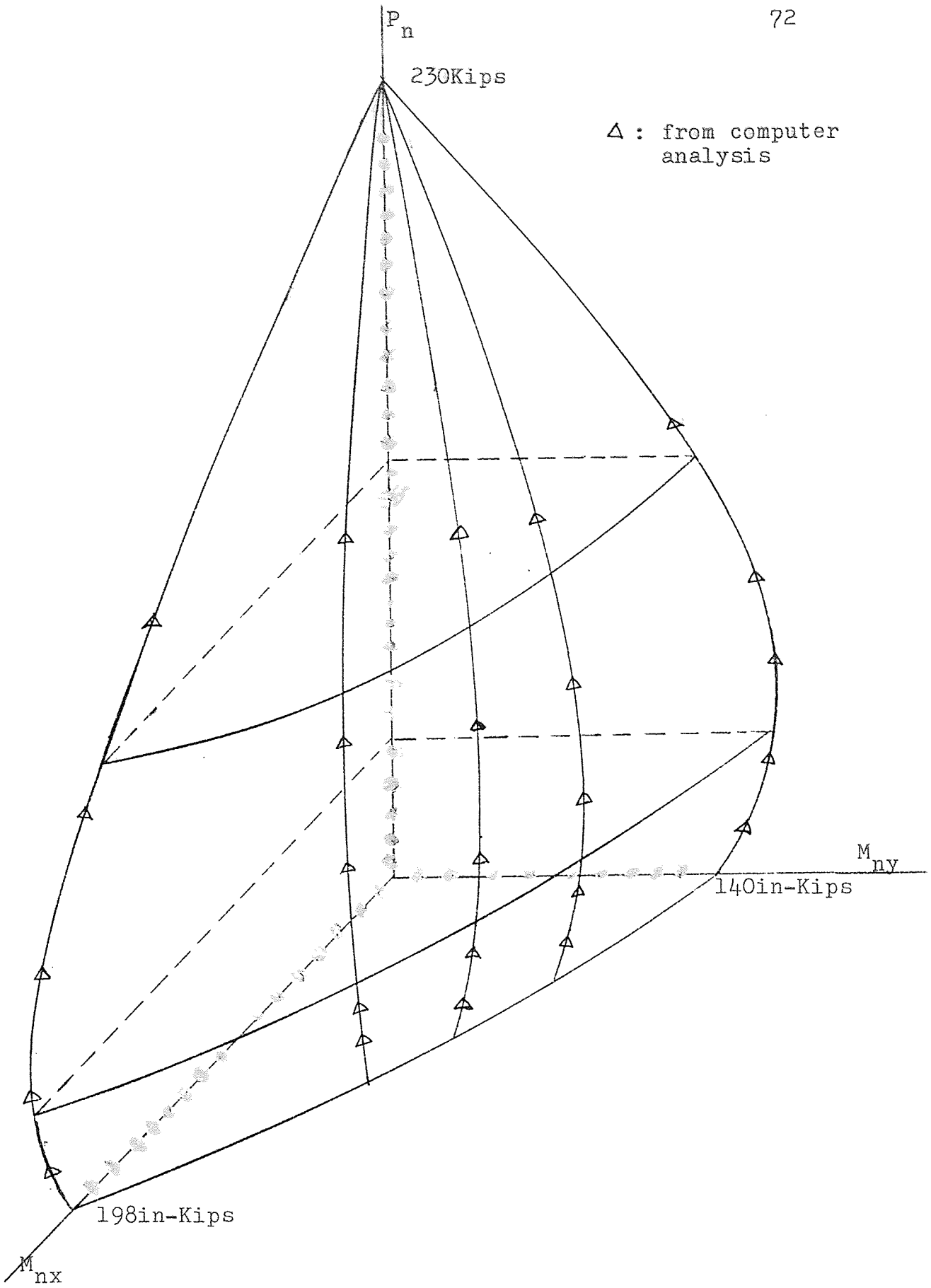

Fig. 4-2-2 FAILURE SURFACE FOR f_c' = 5000 psi

the failure surfaces, the writer compares the theoretical results with the experimental tests as shown in 4-2-1 for f_c' = 3500psi..

In Fig. 4-2-1 point A is the experimental result for monotonic loading (test #4) and point B is the experimental result for cyclic loading (test#9). Both of these two points are inside the failure surface. The reasons are: (1) Different tie spacing (S = 2 in. for computer analysis and S = 3 in. for experimental work). (2) Different maximum concrete compressive stress (f_c' = 3500psi. for computer analysis, f_c' = 3756psi. for test #4 and f_c' = 3868psi. for test #9). (3) Midheight deflection are not included in computing the bending moment for both test #4 & #9. (4) Computer analysis uses the accurate eccentricities than those of the experimental work. However, for point A is only 10% different from the failure surface. This difference can be accepted for design purpose.

CHAPTER V

CONCLUSIONS

As was mentioned earlier, the interaction diagrams and failure surface of L-shaped rienforced concrete columns are the main purpose of this study. The other purpose of the investigation reported here is to study the non-linear deformation behavior of reinforced concrete members subject to biaxial or uniaxial bending moment combined with the axial compression.

A numerical analysis and computer program developed by Hsu for reinforced concrete member subject to biaxial bending and axial load has been used. By using this computer program, the interaction diagrams and the failure surface of biaxial bending and compression are developed for this study.

Some previous design methods by other investigators on column design for combined bending and compression are discussed. A comparison between the computer analysis and experimental work is furnished by using the moment-curvature diagram, three-dimension failure surface, and the interaction diagrams.

The comparison between the analysis and experimental tests are in a satisfactory agreement. The only obvious difference is that of the nondimensional load contours which do not come out the same for rectangular and square sections. Theoretically, the exponent α is dependent only on the cross-sectional properties. Since this thesis is only a preliminary study of interaction diagrams and failure surface for L-shaped reinforced concrete columns, further studies can be conducted in many ways. For example, the length effects can be considered. Meanwhile, more experimental work can be done for comparison.

The results of this investigation are summarized as follows:

(1) The failure surface and interaction diagrams for an L-shaped member subject to biaxial bending and axial compression is discussed and illustrated in chapter 3. The shape of failure surface for an L-shaped cross-section is similar to that of a rectangular section. It is recommended that further studies of deviation of failure surfaces should be conducted.

(2) Bresler's design concept for a member subject to biaxial bending and axial compression can be modified for an L-shaped cross-section.

(3) All these investigations do not consider the buckling of the member. It is recommended that further studies including length effects for L-shaped cross-sections should be conducted.

BIBLIOGRAPHY

1. ACI Committee 318, "Building Code Requirements for Reinforced Concrete (ACI 318-77)", (Detroit: American Concrete Institute, 1977).

2. ACI Committee 318, Design Handbook, In Accordance with the Strength Design Method of ACI 318-77 Vol. 2, Columns, (Detroit: American Concrete Institute, 1978).

3. Concrete Reinforcing Steel Institute, CRSI Handbook, (Chicago: CRSI, 1979).

4. George Winter and Arthur Nilson, "Design of Concrete Structures", 9th Edition, (New York: McGraw-Hill, 1979).

5. Phil M. Ferguson, Reinforced Concrete Fundamentals, 4th Edition, (New Yourk: John Wiley & Sons, 1979).

6. P. Rice and E.S. Hoffman, Structural Design Guide to the ACI Building Code, 2nd Edition, (Van Nostrand Reinhold, 1979).

7. Joaquin Marin, "Design Aids for L-shaped Reinforced Concrete Columns", ACI Journal, Proceedings, 76, November 1979, PP. 1197-1215.

8. C.K. Wang and Charles Salmon, "Reinforced Concrete Design" 3rd Edition, (New Yourk: Harper & Row Publisher, 1979), PP. 451-469.

9. T. Paulay, "Design Aspects of Shear Walls for Seismic Areas",Canadian Journal of Civil Engineering, V2, No.3, Sept. 1975, PP. 321-344.

10. Robert Park and T. Paulay, "Reinforced Concrete Structures", (New Yourk: John Wiley & Sons, 1975), PP. 133-135.

11. Boris Bresler, "Design Criteria for Reinforced Columns under Axial Load and Biaxial Bending", ACI Journal, Proceeding, 57, November 1960, 481-490.

12. Cheng-Tzu Hsu and M.S. Mirza, "Structural Concrete Biaxial Bending and Compression", TN Journal of the Structural Division, ASCE, Feb. 1973, PP. 285-290.

13. Chen-Tzu Hsu, "Behavior of Structure Concrete Subjected to Biaxial Flexure and Axial Compression", (Ph.d. Thesis, McGill Univ., 1974).

14. Cheng-Tzu Hsu and M.S. Mirza, "An Experimental-Analytical Study of Complete Load-Deformation Characteristics of Concrete Compression Members Subjected to Biaxial Bending", Preliminary Report, International Association of Bridge and Structural Engineering, V. 16, Aug. 1974, PP. 45-52.

15. Cheng-Tzu Thomas Hsu and M.S. Mirza, "Non-linear Behavior and Analysis of Reinforced concrete Columns under Combined Loadings", Proceedings of CSCE-ASCE-ACI-CEB International Symposium on Nonlinear Design of Concrete Structures, Aug. 1979, 35 pages.

16. Cheng-Tzu Thomas Hsu, "L-shaped Reinforced Concrete Column Section", Proceedings of the ASCE Engineering Mechanics Specialty Conference, West Lafayette, Indiana, May 23-25, 1983.

17. C.T.T. Hsu, M.R. Taghehchian and M. Yeckta, "Inelastic Behavior of L-shaped Reinforced Concrete Columns", Proceedings of the 9th Canadian Congress of Applied Mechanics, Saskatoon, Canada, May 30-June 3, 1983.

18. F.N. Pannell, "Failure Surfaces for Members in Compression and Biaxial Bending", ACI Journal, Proceedings, 60, January 1963, PP. 129-140.

19. Richard W. Furlong, "Ultimate Strength of Square Columns under Biaxially Eccentric Loads", ACI Journal, Proceedings, 57, March 1961, PP. 1129-1140.

20. J.L. Meek, "Ultimate Strength of Columns with Biaxially Eccentric Loads, ACI Journal, Proceedings, 60, August 1963, PP. 1053-1064.

21. L.N. Ramamurthy, "Investigation of Ultimate Strength of Square and Rectangular Columns under Biaxially Eccentric Loads", Symposium on Reinforced Concrete Columns (SP-13), Detroit: American Concrete Institute, 1966, PP. 263-298.

22. Alfred L. Parme, Jose M. Nieves, and Albert Gouwens, "Capacity of Reinforced Rectangular Columns Subject to Biaxial Bending", ACI Journal, Proceedings, 63, September 1966, PP. 911-923.

23. W.B. Cranston, "A Computer Method for the Analysis of Reinforced Concrete Columns", Cement and Concrete Association, London, Report TRA/402, April 1967.

24. G. Gurfinkel, "Analysis of Footing Subjected to Biaxial Bending", Journal of Structural Division, ASCE, V. 93 No. ST6, June 1970, P. 1049.

25. G Gurfinkel and A. Robinson, "Determination of Strain Distribution and Curvature in Reinforced Concrete Section Subject to Bending Moment and Longitudinal Load", ACI Journal, Proceedings 64, No. 7, July 1967, P. 398.

26. M.R. Taghehchian, M. Yekta and A. Majlesi, "Experimental Investigation of R.C. L-shaped Members under Combined Biaxial Bending and Axial Compression", Unpublished M.S. Report, NJIT, May 1982.

27. Mahmood Saeedi and Azim Meshkooti, "Experimental Investigation of R.C. L-shaped Members under Combined Biaxial Bending and Axial Compression (cyclic loading)", Unpublished M.S. Report, NJIT, May 1982.